UNIVERSITÀ
DEGLI STUDI
DI PADOVA

Head Office: Università degli Studi di Padova

Department of Molecular Medicine

Ph.D. COURSE IN: MOLECULAR MEDICINE
CURRICULUM: BIOMEDICINE
SERIES 36°

LIQUID BIOPSY IN UVEAL MELANOMA:

PROTEOMICS OF AQUEOUS HUMOR

Coordinator: Prof.ssa Arianna Loregian
Supervisor: Prof.ssa Veronica Macchi
Co-Supervisor: Prof. Raffaele Parrozzani

Ph.D. student: Dott.ssa Giulia Midena

SUMMARY

1. ABSTRACT

Background: Posterior uveal melanoma (UM) is the most common primary intraocular malignancy in adults. Primary tumor can be successfully treated, but unfortunately prevention and treatment of the metastatic disease are still unsolved. Clinical, histopathologic and genetic features have been identified as indicators of UM prognosis. However, the mechanisms of UM progression and metastasis are still unknown. In particular, an inflammatory microenvironment has been associated with the presence of high risk histological and genetic characteristics. Moreover, almost all UM carry a driver genetic mutation in a GNA family gene, including GNAQ. Specific genetic features associated with metastatic disease include loss of chromosome 3 and mutations in BAP1 and SF3B1, whereas UM with a mutation in the EIF1AX gene infrequently metastasize. Furthermore, the conservative treatment of UM can cause several side effects and the main involve retinal and choroidal tissue. The term radiation chorioretinopathy encompasses ischemic and nonischemic changes of the choroid and the retina, including the macula (radiation maculopathy). Actually, no biological biomarkers are currently available to identify, in a preclinical phase, subjects at risk to develop radiation macular edema (RME). Notably, UM occurs in a closed microenvironment characterized by a direct contact with ocular fluids. Therefore, the analysis of these fluids may allow to search and identify specific biomarkers providing information about the different pathways involved in UM pathogenesis and in the retinal complications related to its conservative treatment. Aqueous humor (AH) evaluation may represent the most effective and safest liquid biopsy approach in UM.

Aim: To evaluate, *in vivo*, the presence of specific AH biomarkers in eyes affected by UM before and after the conservative treatment.

Materials and Methods: Seventy-two eyes affected by primary UM underwent full ophthalmic examination, including: ophthalmoscopy, fundus

photography, ultrasonography and Spectral Domain Optical Coherence Tomography (OCT). During brachytherapy (Iodine-125) surgical procedure, AH sample collection and 25-gauge transscleral fine needle aspiration biopsy (FNAB) of the primary tumor were performed. AH samples were analyzed to detect the concentration of selected proteins. Cytologic material underwent fluorescence in situ hybridization for chromosome 3. Tumor thickness and largest basal diameter (LBD) were quantified. Tumors were staged using the 8th AJCC classification. The presence of peritumoral serous retinal detachment was categorized considering the number of retinal sectors involved. The same seventy-two UM subjects underwent AH sampling at the time of a planned para surgical procedure 20 months after brachytherapy. The AH of thirty-six normal eyes, scheduled for cataract surgery, was used as control.

Results: Compared with the control group, significantly higher levels of SSTR1 (p=0.028), HMB45 (p=0.018), IL-6 (p=0.047), IL-8 (p=0.008), RANTES (p=0.008), PEDF (p=0.048), Osteopontin (p=0.048), EGF (p=0.041), bFGF (p=0.019), MIF (p=0.009), MCP-1 (p=0.023). VEGF concentration between the two groups was statistically borderline (p=0.058). Comparison between clinical characteristics and cytokine concentrations showed a positive correlation between tumor thickness and IL-8 (p=0.032), and degree of serous retinal detachment and IL-6 (p=0.021). Monosomy 3 was detected in 20 cases (57%) and disomy 3 in the remaining 15 cases (43%). No correlation was found between chromosome 3 status and tumor dimensions (thickness: p=0.301; LBD: p=0.321), and between monosomy 3 and tumor location (ciliary body: p=0.871, choroid: p=0.931). Compared to UM with disomy 3, significant higher levels of IL-6 (p=0.022) IL-8 (p=0.003), RANTES (p=0.005), EGF (p=0.018), bFGF (p=0.012), VEGF (p=0.026), MIF (p=0.005) and MCP-1 (p=0.005) were detected in UM with monosomy 3. Comparison between clinical characteristics of UM with monosomy 3 and cytokine concentration showed a positive correlation between: tumor thickness and IL-8

(p=0.022), tumor thickness and VEGF (p=0.031), LBD and RANTES (p=0.015), and degree of retinal detachment and IL-6 (p=0.021). Compared with the control group, significantly higher protein levels of: GNAQ (p=0.022), BAP1 (p=0.013) and SF3B1 (p=0.023) were detected in eyes with UM. Cluster analysis of UM group revealed 2 clusters, one showing higher expression of GNAQ and BAP1 protein and one of EIF1AX protein. Moreover, the 2 clusters corresponded with the chromosome 3 status of UM. the AH of the UM group 20 months after the treatment showed that 22 subjects (30.5%) developed RME. All RME eyes at OCT analysis had significant increase in thickness of inner and middle retinal layers (p=0.002) mostly determined by intraretinal fluids, in number of hyperreflective retinal foci (p=0.003) and in areas of disrupted external limiting membrane (p=0.004). GFAP, Kir 4.1 and all inflammatory biomarkers were dramatically increased in RME eyes compared to those without RME (p=0.035, p=0.021 and p=0.032, respectively).

Conclusions: Specific and selected proteins may be detected in the AH of eyes affected by UM. These novel findings confirm the possibilities provided by AH analysis in UM before and after its treatment.

2.INTRODUCTION

Nowadays, precision medicine is an emerging concept that stratifies patients and their disease using an array of individual data, including: clinical information, genetics, imaging techniques, biomarker information and multi-omics studies, thus going beyond the observable and classical approach[1, 2]. Therefore, the main goal is to enable more precise targeting of diseases and the best available care for each individual. Within ophthalmology, current efforts are directed at defining the role of intraocular fluids for the development of advanced tools such as biomarkers identification, really helpful in the perspective of precision medicine[3-6]. Therefore, this research is focused on aqueous humor (AH), as the ocular liquid biopsy approach, in posterior uveal melanoma and in the complication related to its conservative treatment.

1.1 THE EYE

The eye is a sense organ specialized in vision. Multiple causes may damage the eye as: trauma, infectious, inflammatory and degenerative disease. Moreover, it can be dramatically involved in systemic disease, even before other relevant systemic localizations or signs appear. Further, the different eye tissues can give rise to several neoplastic diseases[7-9].

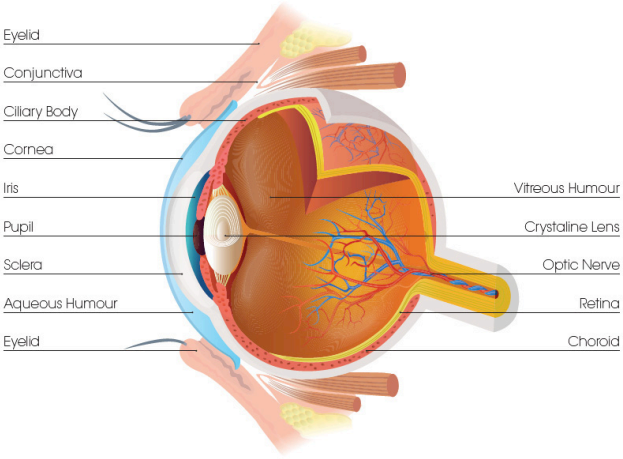

Figure 1. Eye Anatomy.

2.1.1 Anatomy

Each eye is located in the anterior orbit and occupies one-fifth of the orbital cavity. The eye is not a perfect sphere, but it consists of two modified spheres fused together. The anterior, the cornea, has a smaller radius (7.8 mm) than the posterior, the sclera (12 mm). Their junction, the limbus, is marked at the surface by the external scleral sulcus. It is widest at its anteroposterior diameter (24 mm), and is flattened both in its vertical (23 mm) and horizontal (23.5) diameter[7, 8, 10, 11].

The eye is composed by three concentric layers, surrounding the transparent media[7, 8, 10, 11].

Corneoscleral Envelope

The external layer is composed by the cornea and the sclera. The cornea, the anterior sixth, is completely transparent, while at posterior five-sixths, the sclera, is white and opaque, due to the tough coat of connective tissue. The junction between the cornea and the sclera is the limbus. The limbus is the origin for the tissues overlying the anterior sclera, including the bulbar conjunctiva, Tenon's capsule, and the episclera. The latter two of these extend posteriorly and envelop the entire sclera to the point of departure of the optic nerve[7, 10, 11].

Uvea

The middle layer, the uvea, is a high vascular tissue. It consists from behind forwards of the choroid and ciliary body, and the iris. Clinically, the uvea is divided into the anterior uvea and the posterior uvea. The anterior uvea is composed of the iris and the ciliary body. The iris serves as the variable optical diaphragm in the visual system, controlling the entry of light through the pupil. The ciliary body rings the interior of the eye, posterolateral to the iris and surrounding the lens. From the ciliary body, a set of anchoring fibrils, called the zonules, suspend the lens behind the pupil. The posterior uvea is composed of the choroid, a very vascularized layer that provides metabolic support for the outer half of the retina. The

anterior and posterior uvea meet at the ora serrata, which is the visible line of separation between the retina and the posterior edge of the ciliary body. The iris separates the anterior chamber (anteriorly) from the lens and its suspensory ligament behind. Behind the iris and surrounding the equatorial region of the lens there is the posterior chamber, continuous through the pupil with the anterior chamber. Aqueous humor, secreted by the ciliary body, flows into the posterior chamber, through the pupil and out of the globe through a drainage apparatus at the angle of the anterior chamber. The space behind the lens and ciliary body, and within the concavity of the retina, is filled with the vitreous[7, 10, 11].

Particular attention deserves the choroid. Its anterior boundary is the ora serrata and posteriorly it ends around the optic nerve head. The choroid is thickest beneath the fovea (0.3 mm) and thinnest at the ora serrata (0.1-0.15 mm). It is supplied by the short posterior ciliary arteries, but also by the long posterior vessels, which traverse it in the nasal and temporal horizontal meridians. Venous blood drains by multiple tributaries into several vortex veins. The vortex veins traverse a scleral canal and drain into the orbital veins, of which the chief is the superior ophthalmic, that enters the cavernous sinus through the superior orbital fissure. The long ciliary nerves and arteries pass forwards together in the horizontal meridian. Before reaching the suprachoroidal space they occupy discrete scleral canals separated by a thin septum. The nerve usually splits into two within its canal and the artery lies between the division, above the larger part on the nasal side, and above the smaller on the temporal side[7, 10-12]. The layers of the choroid coat are:

1) an external layer of large vessels (Haller's layer);
2) a middle layer of vessels intermediates in size (Sattler's layer);
3) an internal layer of fenestrated capillaries, the choriocapillaris, intimately related to Bruch's membrane.

All these vessels lie in a loose matrix of connective tissue rich in melanocytes, and permeated by nerve fibres.

4) Bruch's membrane, about 2 μm thick, is formed by the basal laminae of the choriocapillaris and retinal pigment epithelium with an intervening zone of collagen and elastic tissue. It provides a barrier restricting movement of large molecules from the choroid. It is rich in collagen, but also contains a middle elastic zone.

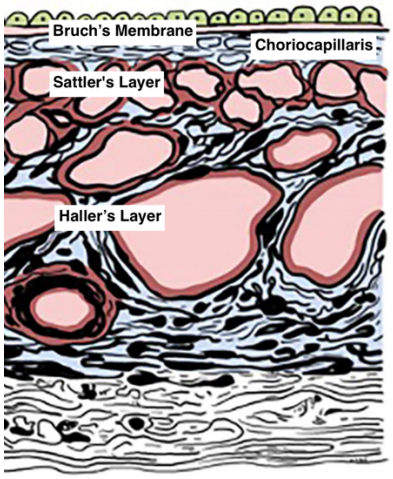

Figure 2. Choroidal layers.

Retina

The inner layer of the eye is composed by the retina. The retina is divided into the neural (sensory) retina and the retinal pigment epithelium[10, 11]. The neuroretina is composed of five main types of neuronal cells (ganglion, bipolar, horizontal, amacrine and photoreceptor cells), glial cells (Müller cells, astrocytes and microglia) and vascular cells (pericytes and endothelial cells)[7, 8, 13]. Between the photoreceptor cells and the underlying choroid there is a single layer of pigmented epithelial cells that assist in nourishing the outer retina, the retinal pigment epithelium (RPE). The main clinical landmarks of the retina include the optic disc, the central retinal artery and vein, and the slightly darker area temporal to the optic disc known as the macula. At the center of the macula resides a shallow depression containing the fovea centralis[7, 8, 10, 11].

Because of the uniform organization of its cellular elements, the retina has an apparent layering, from outside to inside, as follows:

1) pigment epithelium;
2) photoreceptor layer (outer and inner segments);
3) the outer limiting membrane;
4) the outer nuclear layer, containing nuclei of photoreceptors;
5) the outer plexiform layer;
6) the inner nuclear layer, containing nuclei of bipolar cells, horizontal cells, amacrine cells and Muller cells;
7) the inner plexiform layer;
8) the layer of ganglion cells, containing their somas;
9) the layer of nerve fibre axons of ganglion cells;
10) the inner limiting membrane.

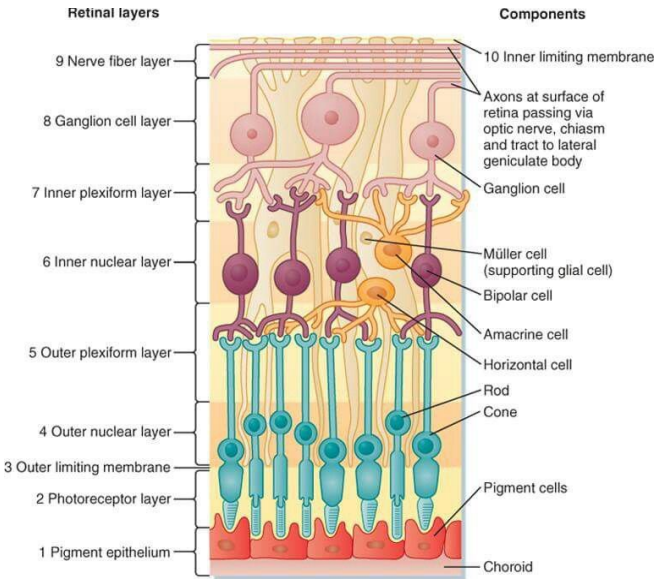

Figure 3. Retinal Layers.

The retinal glial cells comprise the macroglia, which in turn comprises the Müller cells and astrocytes, and the microglia[7, 8, 10, 11, 13]. They function as neuronal structural support cells and represent connection elements between the neurons and the vascular cells, regulating neuronal nutrition, development and metabolism[14]; they contribute, moreover, to the local inflammatory response. Consequently, the glia, even if it

represents only one cellular component of the retina, can influence the physiology of neurons and retinal vessels[11, 13-15].

Macroglia

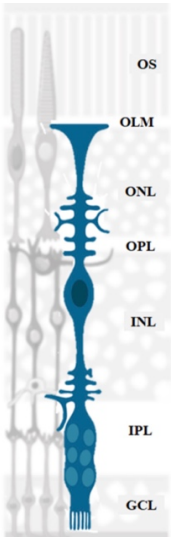

Figure 4. Muller Cell. OS: outer segment; OLM: outer limiting membrane; ONL: outer nuclear layer; OPL: outer plexiform layer; INL: inner plexiform layer; IPL: inner plexiform layer; GCL: ganglion cell layer.

Müller cells, represent the main glial component of the retina and they extend almost through its entire thickness, from the photoreceptor inner segments to the interface with the vitreous[16]. They fill out almost the entire extracellular space between the neuronal elements, and they constitute a great part of the total retinal volume, enveloping and separating different neurons[11, 13, 15, 17]. Their cellular bodies, located in the inner nuclear layer (INL), develop two fibers: one directed towards the outside and one directed towards the inside. The first one, developing lateral processes which branch out in the outside plexiform layer (OPL), ends in the external limiting membrane (ELM), from which it develops microvilli in the space between the inner segments of rods and cones; their function is to increase the cellular surface and to regulate the exchanges of metabolites and ions between the cells and the subretinal space[13, 17]. The second fiber extends into the retinal nerve fiber layer

(RNFL), terminating in a process which comes into contact with the limiting glial cells in order to form the inner limiting membrane (ILM) between the retina and the vitreous humor[13, 17]. Müller cells are connected to blood vessels, astrocytes and neurons, and through the fusion of the basal lamina with perivascular cells and the vascular endothelium, they concur in both composition and function of the blood-retinal barrier[11, 13, 15]. Moreover, they express several ion channels and co-transporters which rapidly remove ions, carbon dioxide and other metabolites released by neurons into synaptic spaces, which determines the association between neuronal activity and blood flow regulation. These cells maintain the stability of the retinal extracellular space and cell plasma membranes through the regulation of retinal ion concentration (in particular potassium), the deactivation and the recycling of neurotransmitters, detritus removal, the regulation of glucose uptake, the glycogen storage and its conversion into lactate, the participation in the glutamate/glutamine cycle and the protection from glutamate excitotoxicity, and the retinoic acid synthesis starting with retinol[11, 13, 15]. Finally, they contribute to the development, metabolism and synaptic functioning of neurons, as well as to the mechanical support and the inflammatory response of the retina[11, 13, 15, 17].

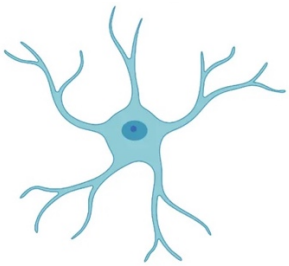

Figure 5. Astrocyte.

Astrocytes, so called due to their star-shaped appearance, are ubiquitous components of the central nervous system (CNS). In the retina their cellular bodies are located inside the RNFL, while their processes envelop the neuronal cells of the ganglion cell layer (GCL)[11, 13, 14, 18].

These cells originate in a migratory process starting from the optic nerve, and, maintaining the same function, they constitute support elements for the axons of the ganglion cells[18]. Their association with the blood vessels of the inner retina concur in both composition and function of the blood- retinal barrier. The endfeet of their processes are in contact with the adjacent capillaries. Astrocytes have a significant role in synaptic regulation, glycogen deposition, neurotransmitter capture and inactivation, and they contrubute to the inflammatory response and in the regulation of ganglion axonal growth[13]. Astrocytes contain particular proteins of the intermediate filaments; ate the immature stage they are composed mainly of vimentin, while subsequently these cells become rich in glial fibrillary acidic protein (GFAP)[13]. Moreover, different ionic channels for potassium, sodium and calcium are located on their surface, for maintaining the equilibrium in the extracellular matrix, and they are able to produce proinflammatory cytokines and to replace the damaged nerve tissue[13].

Microglia

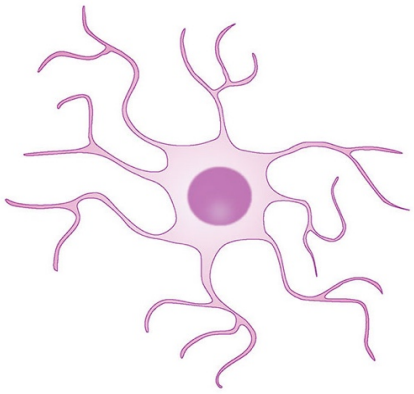

Figure 6. Microglia.

Retinal microglial cells belong to the mononuclear phagocyte system (monocytes-macrophages) which, derived from bone marrow, migrate into central nervous system through blood, representing the most important component of the retinal innate immune system[13, 14, 19, 20]. These cells are located both in the inner plexiform layer (IPL) and the outer one

(OPL), and are endowed with branching processes, usually distributed in parallels on the retinal plane, which give them their star form[13, 15, 20]. Microglia cells usually monitor the extracellular matrix using their processes, but they do not migrate through retinal layers in their rest state; moreover, they come in contact with neural synapses, probably to monitor their functioning. When activated, microglia cells undergo a morphological transformation into amoeboid cells with retracted and thickened branches, alter the expression of their surface molecules and become mobile, migrating into damaged areas of the retina where they participate in the phagocytosis of the degenerating neurons and the cellular detritus, in the secretion of growth factors and cytokines and in the active remodeling of neurons and synapses[13, 20, 21]. Therefore, microglia cells are the main actors to contrast the retinal stress, but if the stress perseveres, they can cause a damaging and persistent inflammatory response[20, 22].

2.2 POSTERIOR UVEAL MELANOMA

2.2.1 Epidemiology

The melanoma of the posterior uvea (choroid) is the most common primary intraocular tumor in adults. It arises from melanocytes in the posterior uveal tract and is commonly named uveal melanoma (UM) [23-25]. UM usually arises from choroidal melanocytes (85%–90%), but can also involve the ciliary body). The median age of diagnosis is approximately 62 years; however, the peak range for diagnosis is between 70 and 79 years[23, 24].

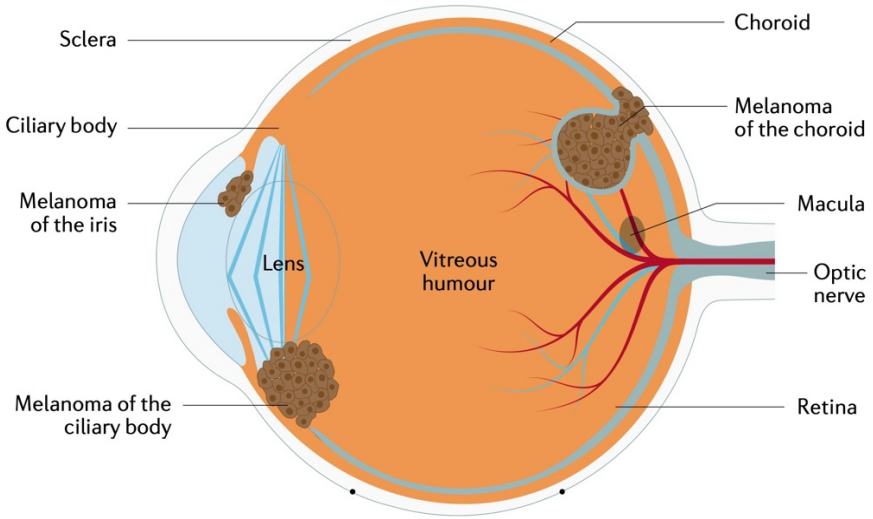

Figure 7. Uveal melanomas (UM) arise from melanocytes in the pigmented uveal tissues.

UM incidence varies by sex, race, and country. Males have a 30% greater incidence than females. In the US, the incidence is approximately five per million individuals, with a significantly higher incidence in non-Hispanic whites (6.02 per million) when compared with blacks and Asians (0.31 and 0.39 per million, respectively). Incidence in Hispanics is around 1.67 per million. In Europe, incidence increases with latitude, ranging from two per million in Spain and Italy, to four to six per million in Central Europe, and greater than eight per million in Denmark and Norway. The incidence in South Korea is similar to Asians in the US: 0.42 per million[26, 27].

At the time of diagnosis, less than 2% of patients have metastatic spread, but once secondary lesions develop, mortality is higher than 95% in the following six months. About 50% of patients affected by UM develop metastases within 2.5 years from the original diagnosis. Metastases are found more frequently in the liver, but also in the lungs, skin and central nervous system; this percentage is unfortunately remained unchanged throughout the last century despite the progress made in recent years both in the diagnosis and in the local control of UM[23, 27, 28].

2.2.2 Pathophysiology

Highly recurrent mutations in UM strongly support the notion that subsequent malignant transformation in uveal melanocytes is driven by the combination of two main events[23, 29]. These events are an alteration in the Gαq pathway and a BSE event (standing for BAP1, SF3B1 and EIF1AX mutations). The real order of oncogenic events that lead to the development of UM is on the way to be elucidated. A mutation in a GNA family gene is suspected to be the initiating event. Furthermore, sophisticated recent genomic analyses support an alternative model of punctuated evolution, with almost simultaneous emergence of all oncogenic events[23, 30].

2.2.3 Diagnosis

The diagnosis of UM is based on clinical examination (slit lamp fundus biomicroscopy and indirect ophthalmoscopy) together with ultrasonography of the eye. UM can be missed unless the fundus is meticulously examined after full pupillary dilatation. Digital photography is most useful for documenting tumor size and location. When a choroidal tumor is large or peripheral, ultra-widefield fundus cameras are especially helpful.

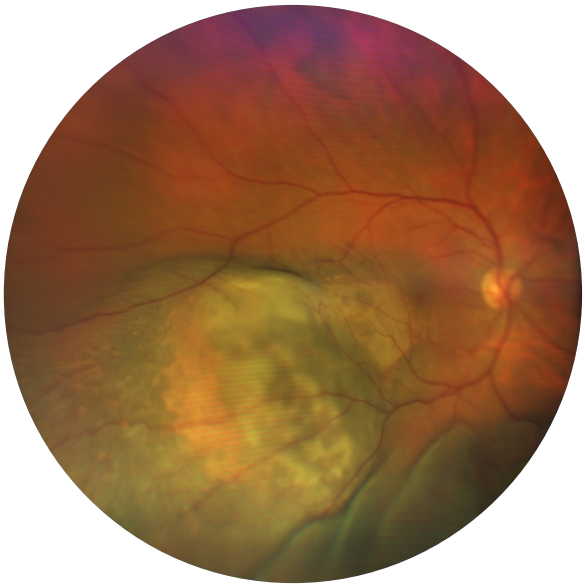

Figure 8. Color fundus photograph showing choroidal UM.

UM are usually flat to dome in shape. Exudative retinal detachment develops early and may eventually hide the tumour when located in the periphery of the retina. Subsequently, the tumor breaks through Bruch's membrane and acquire an essentially pathognomonic mushroom shape. If the tumor additionally infiltrates the retina and vitreous, vitreous bleeding characteristically develops[31]. UM displays classically low reflectivity in A- and B-scan ultrasonography. In A-scan, the spikes are initially high but steadily diminish toward the sclera. In B-scan, the tumour appears dark and acoustically hollow. The reflectivity is less than that of the surrounding choroid, which gives the impression of a choroidal excavation at the base of the tumour[23, 32].

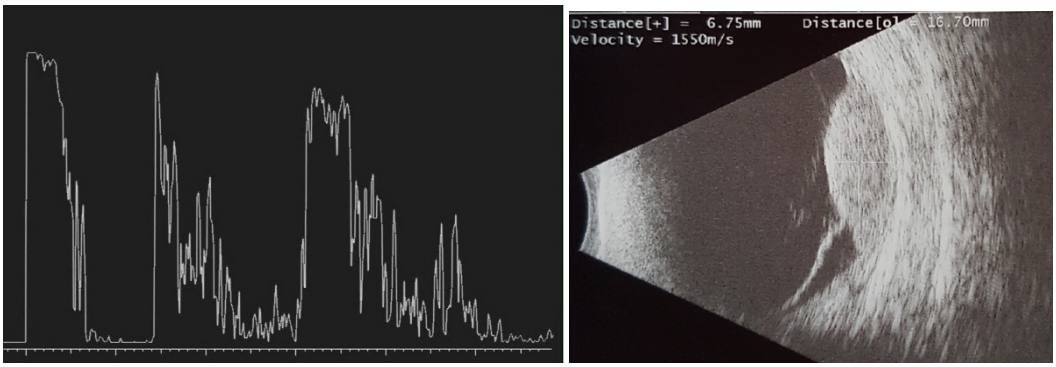

Figure 9. A- and B-scan ultrasonography of UM.

Fundus autofluorescence imaging and optical coherence tomography are helpful in diagnosing small and posterior UM, and the fluid (perilesional serous retinal detachment) around it[33].

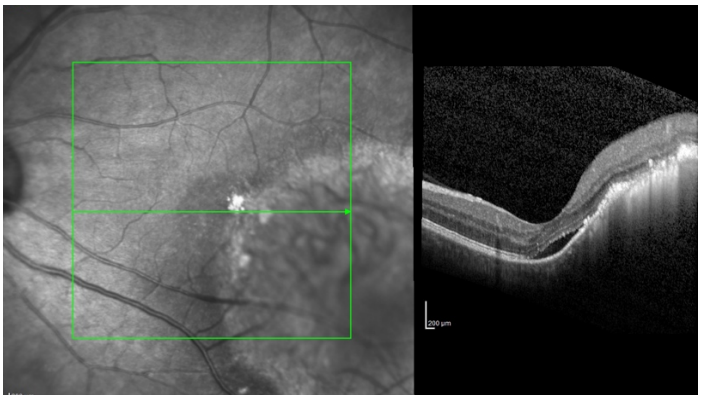

Figure 10. Optical Coherence Tomography image showing subfoveal perilesional fluid.

2.2.4 Staging

The 8th edition of the AJCC (American Joint Commission of Cancer) staging manual uses the tumor, node and metastasis (TNM) model for anatomical staging. In this system, the extent of the primary tumor (T), presence or absence of lymph node involvement (N), and presence or absence of distant metastasis (M) provides information on disease entity and spread. For posterior UM, T is categorized based on tumor basal dimension and thickness into four increasing size classes, including T1, T2, T3, T4 as reported in Table 1[34].

Table 1. AJCC tumor (T) classification of uveal melanoma (primary choroidal and ciliary body melanoma) defined by basal diameter and tumor thickness.

Thickness (mm)							
> 15	4	4	4	4	4	4	4
12.1-15	3	3	3	3	3	4	4
9.1-12	3	3	3	3	3	3	4
6.1-9	2	2	2	2	3	3	4

3.1-6	1	1	1	2	2	3	4
< 3	1	1	1	1	2	2	4
	≤ 3	**3.1-6**	**6.1-9**	**9.1-12**	**12.1-15**	**15.1-18**	**> 18**
	Largest Basal Diameter (mm)						

Secondarily, T is classified according to specific anatomic extent regarding ciliary body involvement and extrascleral extension using categories from "a" to "e", as reported in Table 2[34].

Table 2. AJCC tumor (T) sub-classifications defined by anatomical extent of the tumor based on ciliary body and/or extrascleral involvement.

Tx	**Anatomical extent**
Ta	*without* ciliary body involvement and *without* extraocular extension
Tb	*with* ciliary body involvement, but *without* extraocular extension
Tc	*without* ciliary body involvement but *with* extraocular extension <5 mm in largest diameter
Td	*with* ciliary body involvement and *with* extraocular extension <5 mm in largest diameter
Te	Any tumor size category *with* extraocular extension >5 mm in largest diameter

The regional lymph nodes are assessed by NX (cannot be assessed), N0 (lymph node metastasis absent), and N1 (lymph node metastasis present). Similarly, distant metastases are assessed according to: MX (cannot be assessed), M0 (distant metastasis absent), and M1 (distant metastasis present). When present, M1 is further divided into M1a for metastasis ≤3 cm, M1b for those 3.1-8.0 cm, and M1c for those ≥8 cm. A further refinement in the AJCC classification of UM is the grouping of the individual T, N, and M into Anatomic Staging (Stage I-IV) as reported in Table 3[34].

Table 3. AJCC anatomic stage of uveal melanoma defined by tumor, node, and metastasis values.

Stage	T	N	M
I	T1a	N0	M0
IIA	T1b-d	N0	M0
IIA	T2a	N0	M0
IIB	T2b	N0	M0
IIB	T3a	N0	M0
IIIA	T2c-d	N0	M0
IIIA	T3b-c	N0	M0
IIIA	T4a	N0	M0
IIIB	T3d	N0	M0
IIIB	T4b-c	N0	M0
IIIC	T4d-e	N0	M0
IV	Any T	N1	M0
IV	Any T	Any N	M1a-c

The stages are considered increasingly higher risk for metastasis from Group I to IIA, IIB, IIIA, IIIB, IIIC, and to IV. This staging has yet to be tested with long-term prognostic results. In addition to the above clinical information, identified as cTNM, the AJCC accounts for pathologic information, pTNM, in a similar fashion. The histologic grade is recorded as GX (cannot be assessed), G1 (spindle cell), G2 (mixed cell), and G3 (epithelioid cell)[34].

2.2.5 Treatment of the Primary Tumor

Before the advent of radiation therapy, the elective method in the treatment of UM was eye enucleation. Today, most of the cases are treatable with brachytherapy. This technique has the purpose of bringing the neoplasm first to regression and then to scar atrophy.

Historically, the first application of radioactive material in the treatment of choroidal melanoma is due to Moore who in 1930 used radioactive seeds

of Radon. Subsequently, the seminal work of Stallard and Foster (‘60), followed by Lommatzsch (1974), allowed to develop and standardize the use of Cobalt and Ruthenium plaques in the conservative treatment of choroidal melanoma. Today, the most commonly used isotopes are Ruthenium-106 and Iodine-125, the latter first studied by Packer on animal models in the late 1980s. In 1987, Iodine-125 was chosen as the standard reference isotope within the COMS (Collaborative Ocular Melanoma Study) the first randomized clinical trial comparing brachytherapy to eye enucleation[24].

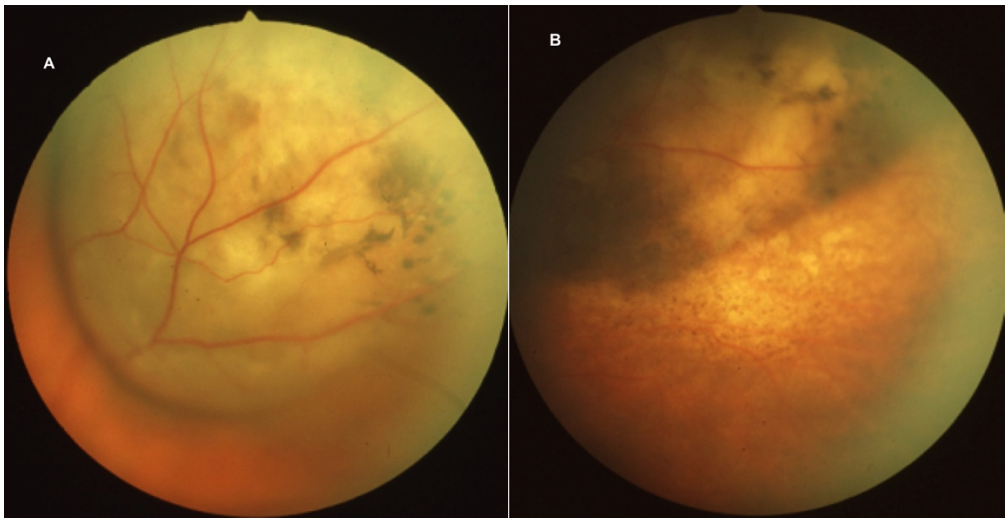

Figure 11. Color fundus photograph showing UM before (A) and after (B) treatment with Iodine-125.

An indirect push towards the development and choice of brachytherapy as the method of choice was provided by Zimmermann, who hypothesized that eye enucleation could be associated with a higher incidence of metastatic disease, stimulating the international community to search for conservative therapies. However, the “Zimmermann’ theory” was never statistically confirmed[35]. The clinical efficacy of brachytherapy depends on offering the affected patient a survival at least equal to that of eye enucleation[35]. The previously mentioned COMS study has definitively demonstrated that patients treated with eye enucleation versus brachytherapy have a statistically similar long-term survival. In addition to

enucleation and brachytherapy, eye irradiation with accelerated particles (protons) and stereotactic radiotherapy are also used in the combined treatment of UM. On the other hand, when liver metastatic disease develops, the therapeutic possibilities are extremely limited. For this reason, growing interest is dedicated to search and validate prognostic factors that may be predictive of a greater risk of dissemination of the primary disease[24, 36]. Some more classic prognostic associations with histological type, size, localization and vascularity are known for some time, others, concerning tumor genetics, are under investigation. Recently the FDA approved Tebentafusp, a bispecific antibody engaging T cells with gp100 on HLA-A*02:01, as the first drug of its class to specifically treat metastatic UM[37].

2.2.6 Prognosis

Despite successful local primary tumor treatment, patients still develop metastases in approximately half of the cases, with a peak at 2.5 years after primary UM diagnosis and therapy. Liver is affected in more than 90% of the cases. Since metastasis occurs even after complete removal of the primary tumor with enucleation, it is suggested that micrometastases are already present at time of treatment[28, 38]. These micrometastases can grow out to a clinically detectable size even more than 10 years after primary treatment. Overall survival for patients with metastasis is very poor. Very early diagnosis and treatment of metastasis may be obtained by more intensive monitoring of high-risk patients. Therefore, it is very important to stratify patients at high-risk or low-risk to develop metastatic disease. For patients with UM, several prognostic markers are known. These prognostic markers can be divided in clinical, histopathological and genetic markers[23, 29].

2.2.7 Clinical prognostic markers

Patient-Related Prognostic Markers

Prognostication is essential to inform patients about the risk for systemic spread of UM. Males and females are affected equally, however the risk for metastasis remains under debate. The COMS study was performed in more than 8.000 patients and found no difference in survival between men and women[38]. Besides gender, also age at diagnosis is associated with survival. Patient diagnosed at a higher age tend to have a worse prognosis. Moreover, older patients also present with larger tumors. Caucasian people are more at risk for developing UM, however according to a recent study which involved 8100 participants, ethnicity is not associated with the prognosis of UM. Thus, although Caucasians are more at risk for developing UM, the risk for metastasis is not increased[23].

Tumor-related prognostic markers

Besides patient characteristics, also several tumor characteristics have been correlated to patient prognosis. The metastasis-rate varies for tumor location. Patients with choroidal melanoma with ciliary body involvement have the highest risk for metastasis[27]. Besides location, is has been shown that tumor diameter and thickness are both independently associated with survival, in which larger tumors associate with increased risk of metastasis. Local invasion which may occur via aqueous channels, ciliary arteries or nerves, vortex veins or the optic nerve may be associated with prognosis. Extraocular extension can be identified using ultrasonography. An increase in the size of the extension is associated with shorter survival[27].

2.2.8 Histopathological prognostic markers

Whenever tumor material is available, UM can be investigated for several histopathological features[39]. UM can be divided based on two cell types, which are spindle cells and epithelioid cells. Spindle cells exhibit elongated nuclei that may contain eosinophilic nucleoli, epithelioid cells have more polygonal cytoplasm and contain eccentric placed large pleomorphic nuclei and prominent eosinophilic nucleoli. The mixed-cell type melanoma

has variable proportion of spindle and epithelioid cells with a minimum of 10% of any type. The presence of epithelioid cells in the UM is associated with a worse prognosis for the patient[40]. Other intra-tumor factors, like the presence of certain extracellular matrix patterns and increased mitotic figures (number of mitoses per 50 high-power fields) can both provide additional adverse prognostic information[41]. Other histological features associated with mortality and metastases are mean diameter of ten largest nucleoli, degree of pigmentation, presence of inflammation and tumor necrosis. Extrascleral extension by perineural, perivascular, intravascular or direct scleral invasion is correlated with a worse prognosis. Immunohistochemistry may be of diagnostic value. S-100 is expressed by cells of neuroectodermal origin, as uveal melanocytes. Human Melanoma Black-45 (HMB-45) binds to glycoprotein 100 (gp100), an antigen expressed by melanocytes that can be useful in differentiating UM from nonmelanocytic tumors[40]. However, a study of 1527 enucleated eyes conducted by the COMS group revealed that all these histopathological characteristics are not independent but associated with each other[40]. Tumors located in the peripheral choroid of the eye are in general larger, contain more epithelioid cells and more tumor necrosis. Moreover, epithelioid cells in UMs are associated with a higher degree of tumor necrosis, pigmentation and inflammation, and large tumor size. Based on the statistics it is hard to determine which feature precedes the other. It is most likely that tumors located more anteriorly are diagnosed later since these tumors tend to cause less symptoms. Growing tumors without proper vascularization develop necrosis, which recruits inflammatory cells. The hypoxia-induced necrosis can also recruit vascularization and epithelial-to-mesenchymal transition (EMT) factors that promote proliferation and local invasion. This results in a higher metastatic risk[42].
With the increasing knowledge about genetics and the development of next generation sequencing tools to explore tumor specimen, a shift towards genetic determinants of tumorigenesis and risk for metastasis was feasible.

2.2.9 Genetic prognostic markers

Chromosomes

UM is a malignancy characterized by several non-random recurring chromosomal aberrations. “Non-random recurring” means that the tumors in a proportion of the patients contain similar chromosomal aberrations. As each chromosome has two copies, chromosomal aberrations are also named copy number variations (CNVs)[43].

Chromosome 3

Among these non-random recurring CNVs, the loss of the entire chromosome 3 was observed several decades ago in tumor material of UM patients. Loss of chromosome 3 (monosomy 3) is observed in nearly half of the UM, and is to date the most strongly associated CNV with metastases. In UM with monosomy 3, different regions of the tumor were analyzed for chromosome 3 to determine intratumor heterogeneity[43]. This revealed that monosomy 3 UM show loss of chromosome 3 in the entire tumor suggesting that UM with monosomy 3 are quite homogenous. Besides monosomy 3, another chromosomal abnormality that can be observed is isodisomy 3. In these tumors there are two identical copies of chromosome 3, thus resulting in a loss of heterozygosity (LOH). LOH of chromosome 3 is even more predictive for metastasis than monosomy 3[43].

Moreover, it has been demonstrated that the loss of a chromosome 3 is often the earliest alteration associated with the development of UM and that the other chromosomal alterations are related to the loss of a chromosome 3. So, the loss of chromosome 3 is part of a two-step path of carcinogenesis typical of tumor-suppressor genes. In most cases, since the loss of the chromosome is complete, it has been impossible for a long time to trace the gene or genes that once lost were responsible for the malignant transformation[43]. Other genes located elsewhere on chromosome 3 also appear to be involved in the carcinogenesis of UM. In

particular, the FITH gene (fragile histidine triad) and the VHL gene (von Hippel Lindau) seem to be involved in its pathogenesis. Closely related to the loss of chromosome 3 are some alterations of chromosome 8[44].

Chromosome 8q

Another copy number (CN) event is the gain of the long arm of chromosome 8. Gain of chromosome 8q is observed by either entire chromosome 8 gain, the formation of an isochromosome 8q or a partial amplification of the distal end of 8q. The formation of an isochromosome 8q is mainly observed mutually with the loss of chromosome 3 in which the combination of these CN events in the UM are associated with the most rapid systemic progression of the disease[44].

Chromosome 6p

Chromosome 6p gain is present in almost half of the UM and usually observed in tumor samples without chromosome 3 loss. Similar to chromosome 8q, chromosome 6p gain is observed either by an entire gain of chromosome 6, via the formation of an isochromosome 6p or an amplification of the distal part of chromosome 6p. Unlike chromosome 8q, the different types of gain have not been associated with other chromosomal aberrations[45].

Genes

UM harbors mutations in genes that are involved in tumorigenesis. Although most of these mutations are somatic, germline mutations giving rise to the BAP1-syndrome have been described, typically associating malignant mesothelioma and UM development[46].

GNAQ, GNA11, CYSLTR2 and PLCB4

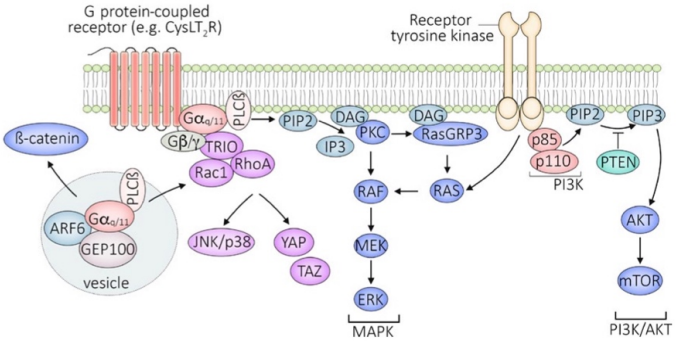

Figure 12. Signaling pathway in UM.

Sequencing of 24 potential oncogenes involved in the RAF/MEK/ERK pathway led to the discovery of a hotspot mutation in GNAQ (Guanine nucleotide binding protein, subunit q; chromosome 9q21.2). This hotspot mutation targeting amino acid 209 (Q209). Within a year the hotspot Q209 mutation in GNA11 (Guanine nucleotide binding protein, subunit 11; chromosome 19p13.3), the homologue of GNAQ, was identified. Mutations in both gene occur in approximately 90% of the UM, were not associated with survival. UM that do not contain a GNAQ or GNA11 mutation usually harbored a mutation in another gene linked to the GNAQ/11 pathway: phospholipase C beta 4 (PLCB4) and cysteinyl leukotriene receptor 2 (CYSTLR2) [23, 29].

BAP1

Whole-exome sequencing (WES) of two samples with a loss of chromosome 3 led to the discovery of inactivating mutations in the tumor suppressor gene BAP1 (BRCA-associated protein 1; chromosome 3p21.1). BAP1 is a ubiquitin carboxy-terminal hydrolase, an enzyme responsible for eliminating ubiquitin from protein substrates[47, 48]. BAP1 was initially shown in the cell nucleus where its primary interaction was binding to the BRCA1 and enhancing its tumor suppressive activity. Subsequently, it has been documented that BAP1 acts independently as a tumor suppressor, using its deubiquitinating activity to regulate proteins involved in cell proliferation, cell cycle control, cellular differentiation, DNA damage repair, chromatin modulation, regulated cell death and immune

response. Unlike GNAQ/GNA11 mutations, BAP1 status of the tumor was strongly correlated with survival[23, 29].

SF3B1

Additional WES of primary UM, led to the discovery of an SF3B1 (Splicing factor 3b, subunit 1, chromosome 2q33.1). SF3B1 mutations also occurred in chronic lymphocytic leukemia (CLL) and myeolodysplastic syndrome (MDS). SF3B1 mutations were strongly correlated to disomy 3 tumors[23, 29].

EIF1AX

Another recurring mutated gene in UM discovered with WES is EIF1AX (eukaryotic translation initiation factor 1A, X-linked, chromosome Xp22.12). Similar to SF3B1 mutations, also EIF1AX mutations were strongly correlated with disomy 3 tumors. EIF1AX mutations occur in approximately 20% of the UM cases, and were only found in the first 15 amino acid (exon 1 and partially exon 2). Also similar to the SF3B1 mutations, the EIF1AX mutations are gain of function mutations result in an intact albeit altered protein. Tumors harboring an EIF1AX mutation are associated with a better survival compared to tumors without EIF1AX mutations [23, 29].

2.2.10 Tumor Microenvironment

The eye is an immune-privileged site, but inflammation can be present within the established ocular tumor microenvironment[49]. Inflammation was recently established as the seventh hallmark of cancer[50]. Cancer cells may exploit immune evasion to survive and expand. UM are quite homogeneous without much stromal tissue and may be the major influence on the influx of tumor-infiltrating leukocytes (TIL)[51]. Inflammatory infiltrates play a critical role during different developmental stages of most malignancies and their progression. It is essential focusing at the several cells present in the tumor microenvironment. With regard to

UM, this infiltrate consists of a heterogeneous group of cells. Not only T cells but also macrophages (that can be identified because they express CD68+) are commonly present in UM and are referred to as tumor-associated macrophages (TAMs)[52]. Their number is higher in tumors with epithelioid cells, increased microvascular density (MVD) and large tumor size, all of which are markers of increased malignancy. The presence of a T lymphocyte infiltrate is usually positively correlated with an increased density of CD11b macrophages, both of which are related to human leukocyte antigen (HLA) expression. This increased expression of HLA class I as well as HLA class II occurred more frequently in epithelioid cell type tumors. Two types of TAMs can be identified: M2 and M1 macrophages. The former generally have less antigen presentation or tumoricidal capacity and show a high expression of angiogenic factors (as vascular endothelial growth factor -VEGF-). On the other hand, classically-activated M1 macrophages kill cancer cells and elicit tumor-destructive reactions centered on blood vessels. In UM, the macrophages within the tumor almost all display the same phenotype, as determined by immunofluorescence histochemistry with monoclonal antibodies against CD68 and CD163, which qualifies them as the M2 type[52].

Immunologic determinants related to prognosis include HLA expression and lymphocyte and macrophage infiltration[53]. Although it was thought that the presence of infiltrating antigen-presenting cells (APCs) would help to stimulate antitumor immune responses, current data suggests that the presence of infiltrating macrophages and T cells is associated with a worse survival. The combined presence of infiltrating macrophages, lymphocytes and an increased expression of inflammation-related molecules (HLA class I and II) is known as the inflammatory phenotype of UM[52, 54].

Genetic events may generate the expression of inflammation-related molecules, leading to the recruitment of myelomonocytic cells and stimulation of angiogenesis. Furthermore, inflammation and cancer may have a mutual influence by contributing to the genetic instability of cancer

cells[55]. UM may acquire chromosomal defects as they grow, such as monosomy 3 or gain of (iso)chromosome 8q, further increasing the risk of metastatic death. The inflammatory phenotype correlates with one specific genomic abnormality. The orchestration of the myelomonocytic cell influx and function differentiation is a key element in pathways connecting inflammation and cancer. In UM, there are several mechanisms where the tumor may take advantage of the inflammatory microenvironment. The immune cells in the microenvironment, macrophages in particular, adopt a trophic role during tumor progression. UM may actively recruit macrophages, with which they synergize to establish the pro-angiogenic, immunosuppressive, and thus prometastatic environment, which downregulates innate and adaptive immune responses[56].

Specifically, the UM microenvironment includes soluble components: cytokines and chemokines that may be derived from either neoplastic or non-neoplastic cells[57]. Cytokines and receptors comprise a large family of molecules that control immune cells during their development[58]. Inflammation is not only localized in the tumor itself, as UM eyes often carry increased levels of inflammation-related cytokines in their AH[57]. Several in vitro studies of UM showed a range of important factors. In one study, melanoma cell lines expressed IL-2R and IL-15R, while tumor-infiltrating lymphocytes and macrophages produced IL-2 and IL- 15 that stimulated tumor cell proliferation. Soluble factors secreted by macrophages influence the production of the melanoma inhibitory activity (MIA) of UM cells[59]. MIA is known to inhibit tumor cell attachment to the extracellular matrix enhancing their invasive potential. Production of MIA by tumor cells increased when macrophage-conditioned medium was added to human UM cell lines. In turn, tumor cells may influence their interaction with macrophages by promoting an M2-like polarization. Macrophage migration inhibitory factor, a cytokine that produces an immediate inhibition of NK cell-mediated lytic activity, is produced by UM cell lines. This NK-inhibiting immune privilege contributes to the growth

and metastasis of ocular melanomas by affecting cytolysis of UM target cells[60].

2.3 LIQUID BIOPSY

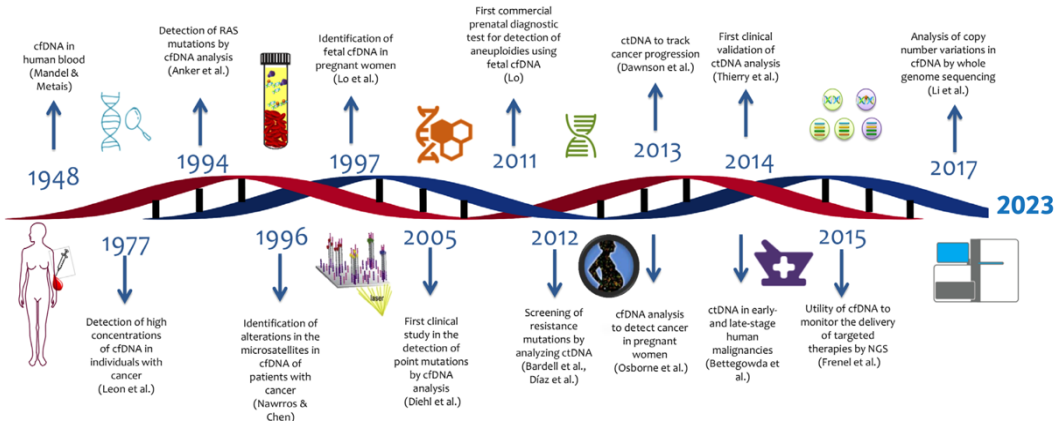

Figure 13. Liquid biopsy evolution.

Tissue biopsy is a common procedure in medicine and in particular in oncology, involving the removal of a sample of tissue for its examination. The limitations to such invasive procedures include difficulty in acquiring tumor samples for both tumor quantity and quality. Moreover, acquiring biopsy samples by invasive methods throughout treatment to monitor tumor response and relapse also poses a major challenge in tumor profiling. Heterogeneity of resected tumor samples as a whole, also limits the use of invasive methods[61, 62]. Additionally, in the case of metastases, when tumors have spread and evolve, both spatially and temporally, in response to treatment, multiple biopsies may be required as it is difficult to obtain a holistic image of a tumor[63]. Considering the challenges associated with traditional biopsies, oncology research has shifted its focus toward analyzing various biological fluids rather than whole tissues for tumor-derived components; a technique referred to as liquid biopsy[61, 62]. Indeed, just over ten years ago the term liquid biopsy was introduced to describe the use of circulating tumor cells as possible tumor biomarkers in breast cancer. Nowadays, according to National

Cancer Institute is termed liquid biopsy: “a test done on sample of blood, urine, or other body fluid to look for cancer cells from a tumor or small pieces of DNA, RNA, or other molecules released by tumor cells into a person’s body fluids”[64]. Indeed, in the liquid biopsy approach are involved circulating subcellular structures, mainly: cell-free DNA, cell-free RNA, circulating tumor cells and exosomes.

Cell-free DNA

The identification of circulating nucleic acids in blood was described for the first time in 1948, although their importance was not considered until later, when cell-free DNA (cfDNA) levels were observed to be increased in cancer patients. Therefore, was demonstrated that some of this cfDNA came from tumor cells and carried their same alterations[65]. Most of the cfDNA in blood are short fragments (range of 145–201bp or multiples of this size) resembling the nuclease-cleaved fragments of DNA packaged into the nucleosomes. Apoptosis seems to be the principal mechanism by which DNA is relased into circulation. A second source of cfDNA are necrotic cells[61, 62]. This occurs more frequently in tumor cells, which have a high necrosis rate due to their hypoxic microenvironment. Finally, another source of cfDNA is the active DNA release into the circulation as it has been observed in cultured human bone cancer cells. CfDNA circulates in blood at a very low concentration (ng/mL) and serum levels are two to four fold higher than plasmatic ones[61, 62]. For this reason, plasma is usually preferred to serum, avoiding the high background level of noninformative cfDNA. Circulating cfDNA has a short half-life as it is rapidly removed from circulation, mainly to liver, spleen, and kidney[61, 62]. Tumor cfDNA can be detected in blood obtained from patients with different kinds of cancer, but with a very drifter concentration, that usually increases with the staging, probably related to the tumor size or load. Newsworthy, mutations detected in cfDNA correlate with those detected in the tumor tissue. Furthermore, cfDNA analysis can provide data related to tumor heterogeneity, information that a tissue biopsy cannot always

provide because it is dependent on the quality and how representative the cancer tissue sampled is. The successive analysis of mutations in cfDNA can be repeated throughout the treatment [61, 62].

Cell-free RNA

For several years, gene expression analysis has been related to protein-coding genes encoding different types of messenger-RNAs (mRNAs). In recent years it has been shown that the main part of the transcriptome of human cells corresponds to noncoding RNAs (ncRNAs), and only 2% of the genome is transcribed into protein-coding RNAs. This finding together with the association of ncRNAs with physiological and different pathological conditions has greatly increased the interest of non-coding molecules in the transcriptional landscape[61, 62]. There are different classifications of ncRNAs due to their genomic orientation, function and location. However, ncRNAs are usually divided into two major groups based on transcript size, with small ncRNAs that are shorter than 200 nucleotides (nt), such as miRNAs, small interfering RNA (siRNA), and piwi-interacting RNA (piRNA); and long noncoding RNAs (lncRNAs) that are longer than 200 nt, including among others, long intergenic ncRNAs (lincRNAs), long intronic ncRNA (intronic lncRNAs), and circular RNAs (circRNA) [61, 62].. The discovery of these noncoding molecules has opened up a whole new field of research leading to the establishment of ncRNA species as fundamental regulators of gene expression and cellular functions. The most studied ncRNAs are miRNAs (18–25 nt) that have important roles at post-transcriptional and translational levels regulating multiple human protein-coding genes. They are involved in regulating different processes, including: proliferation, apoptosis, and development. On the other hand, lncRNAs constitute the vast majority of the noncoding transcriptome. Although lncRNAs lack protein-coding potential, they can display some mRNA-like properties [61, 62]. Although most of the lncRNAs have not been carefully studied yet, a few of these molecules have been well characterized mainly in cancer, acting as oncogenes or as

tumor suppressors. Several studies have demonstrated that ncRNAs are disrupted in different diseases, including tumorigenesis. The causes of this deregulation include genetic events leading to abnormal expression, such as CNVs or single-nucleotide polymorphisms (SNPs) located in ncRNA regions. However, another possibility is that ncRNAs may themselves be targets of epigenetic disruption due to promoter CpG island hypermethylation- associated silencing[61, 62]. Different RNA species are released from human cells and tissues into the body fluids (blood, urine, cerebrospinal fluid, or saliva, among others) representing an enormous filed of research for biomarker discovery. Many studies have focused on ncRNA analysis because they are more stable and detectable in circulation than mRNAs [61, 62]. The detection of circulating tumor-associated mRNAs was first described in the blood of patients with melanoma and then different circulating ncRNA species have been identified in oncologic patients. Since cfRNA profiling of diseases has provided highly valuable information in several studies, they are increasingly recognized as noninvasive and readily accessible biomarkers for diagnosis, prognosis, and therapy response applications. [61, 62]. Furthermore, higher levels of specific miRNAs were associated with diagnosis and prognostic outcome in diffuse large B-cell lymphoma patients, suggesting that miRNAs had potential as clinically useful noninvasive biomarkers. Moreover, several studies have reported the clinical utility of assessing specific miRNAs in different fluids as diagnostic, prognostic, and predictive biomarkers, including in early stages of the disease. In addition to miRNAs, circulating lncRNAs have also shown to be useful in a clinical setting[61, 62].

Circulating Tumor Cells

The presence of circulating tumor cells (CTCs) was first observed by Ashworth in 1869. This is a normal event during malignant tumor development. Primary neoplasia or metastasis releases cancer cells, which intravasate into blood and lymphatic vessels and eventually

disseminate and proliferate at distant sites to form metastases[61, 62]. Nowadays, the presence of CTCs in blood has been demonstrated in several tumors, mainly in breast cancer, and their clinical utility has been deeply studied. As the primary tumor also CTCs can be heterogeneous. Moreover, some of these cells express a EMT, which results in a more mesenchymal or even more stem cell-like phenotype. CTCs are extremely rare in blood and normally only a few CTCs/mL can be detected in peripheral blood. Their diameter is heterogeneous but, in general, larger (20–30μm) than that of white blood cells (8–10μm) and erythrocytes (8 μm), and even larger than the caliber of capillaries (5–10 μm), so it should be expected that most of them would be trapped and only a few of them, would continue circulating. Moreover, the site of blood collection could affect the number of collected CTCs. Tumors can spill off into circulation single tumor cells or clusters of several tumor cells, which can be polyclonal. These clusters of CTCs, although much rarer than single CTCs, have higher metastatic potential. Furthermore, CTCs can associate with platelets and leukocytes. Platelets aggregations facilitate generation of CTCs, as they provide angiogenic signals such as VEGF. Platelet coat also provides CTCs a cloak from natural killer (NK) cells attacks as TGF-β released by platelets downregulates NKG2D in immune cells. Platelets are also involved in CTCs interaction with endothelial cells by means of expressing adhesion molecules both implied in extra/intravasation of CTCs[61, 62].

Exosomes

Exosomes are small microvesicles with a size between 50 and 150 nm secreted by alive cells by an ATP-dependent mechanism. Several sytudies have shown that exosome production is an ubiquitous cellular process. In fact, tumor cells are especially active in secreting exosomes with increased concentrations of tumor-derived exosomes in plasma during cancer progression. Low oxygen tension induces the biogenesis of exosomes by tumor cells. Exosomes derive from the internal vesicles of

the multivesicular bodies and contain nucleic acids (DNA, miRNA, single-stranded RNA, lncRNA), proteins, and lipids. Typically, exosomes contain the endosome-specific tetraspanins (CD9, CD63, and CD81), accessory endosomal sorting complexes required for transport (ESCRT) pathway proteins (ALIX and TS101), proteins involved in membrane transport and fusion (RAB proteins and annexins), cytoskeletal proteins (actin and tubulin), G proteins and adhesion molecules (integrins) [61, 62]. Moreover, exosomes contain other proteins that could serve to identify the cellular source, such as CD14 for monocytes or CD105 for epithelial cells. Finally, tumor-derived exosomes can carry molecules that distinguish them from other circulating exosomes released by nonmalignant cells. Some of the RNA and protein transported in exosomes can be delivered to recipient cell serving as a communication mechanism between cells. Probably, the most noticeable effects are related to stroma modification, angiogenesis, and immunomodulation[61, 62].

The methodological approaches to analyze these biomarkers depend on the specific biomarker studied. Nowadays, liquid biopsy research has undergone an exponential evolution with a fast implementation in clinical practice. Moreover, new actors in a leading role are emerging in the liquid biopsy scenario, therefore this procedure is moving to a multimodal approach with the analysis of proteins that provide new information regarding disease phenotypic information.

Proteins

Protein expression analysis in body fluids might provide information closer to the disease biology than mutation analysis. Therefore, it is essential to address proteomics. Proteomics is a new type of “omics” that has rapidly developed, especially in the therapeutics field. The word proteome was created by Marc Wilkins in 1995[66, 67]. Proteomics is the study of the interactions, function, composition, and structures of proteins and their cellular activities. Proteomics provides a better understanding of the

structure and function of the organism than genomics. It is estimated that there are almost one million human proteins, many of which contain some modifications such as post-translational modifications. There are a variety of proteomics techniques and protein expression mapping can provide an understanding of the post-translational modifications of expressed proteins under different environmental conditions or disease states. Proteomics is a multi-step technique in which every step should be very well controlled to avoid non-biological factors interfering with protein expression and interaction[66, 67]. Sample preparation is the most important step because it solubilizes all proteins in the sample and eliminates all interfering inhibitory compounds such as lipids. Adequate sample preparation is crucial to obtain reliable, accurate, and reproducible results. Proteomics can analyze the expression of a protein at different levels allowing the assessment of specific quantitative and qualitative cellular responses related to that protein. Qualitative and quantitative proteomes are measured at post-transcriptional, transcriptomic, and genomic levels. According to the conditions, qualitative proteomics utilizes microarrays, two-dimensional (2D) gel electrophoresis, and label-free quantification of high mass resolution liquid chromatography to monitor protein mixture composition and protein expression changes. Moreover, it can provide information on the molecular mechanisms of diseases and compare two groups such as patients with healthy controls. Quantitative proteomics can also provide deep insights into disease mechanisms, cellular functions, and biomarker discovery. There are three main types of proteomics: expression proteomics, functional proteomics, and structural proteomics.

Expression proteomics studies the quantitative and qualitative expression of proteins. It aims to specify the difference in protein expression between two conditions such as patients and controls. In addition, it can identify disease-specific proteins and new proteins in signal transduction. Expression proteomics experiments are usually used to study the patterns of protein expression in different cells. Structural proteomics specifies all protein interactions such as membranes, cell organelles, and ribosomes in

the mixture. Functional proteomics studies the protein functions and molecular mechanisms in the cell and determines the protein partner's interactions. In particular, it investigates the interaction of an unknown protein with partners from a specific protein complex involved in a particular process. This may indicate the biological role of the protein. In addition, the elucidation of protein-protein interactions in vivo can lead to comprehensive descriptions of cellular signaling pathways[66, 67].

Therefore, the importance of proteomic-based profiling in cancer liquid biopsies is increased. Since proteins are the direct executors of most cellular functions and the direct drug targets in most current cancer therapies, proteomic data are likely to provide novel insights to aid biomarker identification and clinical implementation. Protein profiles from liquid biopsy samples also likely reveal more organ-specific information than DNA or even RNA, which helps to identify tumor origin. Despite the challenges, the irreplaceable values and clinical demands of novel proteomic biomarkers in cancer liquid biopsies bring ever-growing excitement among researchers to revolutionize technologies to understand the proteome better. In this scenario, break-throughs have been made in recent years with advancement in existing technologies and with the advent of innovative methodologies. One future direction is the development on the technical side of proteomics[66, 67]. With various technological advancements in every aspect, proteomic-based biomarker discovery can be fundamentally redefined in the ballpark of cancer liquid biopsy.

2.3.1 Liquid Biopsy in Uveal Melanoma

Regarding UM, although biopsy of the primary tumor can provide valuable prognostic information, biopsies of intraocular tumors are invasive procedures, with severe complications, including hemorrhage of both tumor and surrounding tissues and retinal detachment[39, 68, 69]. Additionally, although it has been empirically disproved, there is still a risk

about the possibility of intraocular biopsies provoking unwanted systemic tumor cell dissemination. Furthermore, biopsies have been reported to show discordant profiles depending on where tissue is sampled. As such, single biopsies may inadequately sample disease and provide only a snapshot of the tumor; repeated biopsy to monitor changes and tumor heterogeneity is simply not possible[39, 63]. Hence, an easier and less invasive biopsy method to sample the ocular tumor is warranted in UM. This ideal approach should reflect both the status of the primary tumor and the risk or presence of metastasis, monitor the molecular changes that occur as part of the natural history of disease and in response to therapy, be easy to repeat, and be well tolerated and minimally invasive[68, 69]. Therefore, liquid biopsy has emerged as a less invasive alternative that also offers the ability to track genomic changes longitudinally over time. Most liquid biopsy research in UM has focused on the blood as a biofluid source of CTCs[63, 68]. Unfortunately, the prognostic value of CTCs in UM remains unclear, and comparison between studies is difficult due to varying methodologies. Moreover, the clinical use of CTCs is constrained by the difficulty in differentiating tumor-specific CTCs from other cell types in the circulation. Moreover, the low tumor fraction found in the blood due to the blood-ocular barrier limits the detection of prognostic biomarkers; thus, blood liquid biopsies for UM may be better utilized to detect systemic disease[63].

2.3.2 Aqueous Humor Proteomics

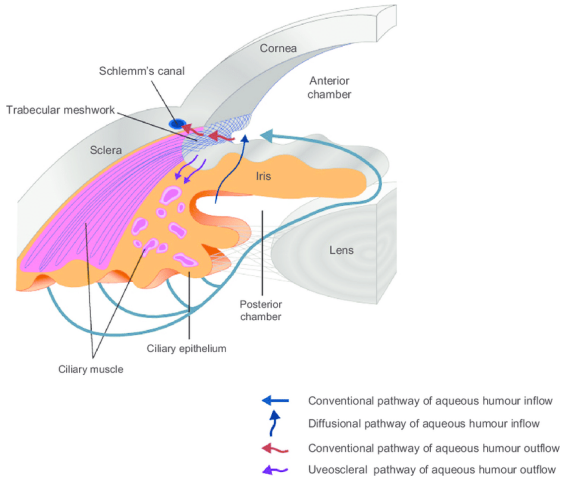

Figure 14: Schematic representation of the hydrodynamics of the aqueous humor. Produced by the nonpigmented ciliary epithelium, it leaves the anterior chamber through the trabecular meshwork and Schlemm's canal and in minimal part through the uvea.

The AH is a clear, transparent liquid located in the anterior and the posterior chambers of the eye: while most of it (the four fifths) is located in the anterior chamber, a fifth is found in the posterior chamber where it is produced by the nonpigmented ciliary epithelium[7, 10, 11]. However, as demonstrated by the qualitative and quantitative differences of proteins, ions and other solutes with respect to the plasma, the AH is not formed exclusively for a simple process of diffusion and filtration, but also for the active secretion operated by intraocular tissues, in particular by the ciliary epithelium. From the posterior chamber, the AH flows into the anterior chamber passing between the iris and the crystalline lens, and from here a major part (85%) is drained, through the episcleral venous plexus (trabecular pathway or the usual one); a small quantity (15%), however, reaches the choroid venous vessels through the uveal trabeculae (sclerouveal pathway) [7, 10, 11].

This ocular fluid plays an important role in maintaining certain functions, (ocular refraction, form and pressure); in addition, it supplies nutritive substances and the oxygen to the cornea, the crystalline lens and the trabecular meshwork, and it removes waste substances; finally, it

contributes to the constitution of the local immune system. From the physical point of view, the AH presents a specific weight which varies from 1003 to 1012, a refraction index between 1132 and 1137, and inferior viscosity and superior surface tension compared to the plasma. From the chemical point of view, AH is composed by a complex mix of electrolytes, organic solutes, growth factors, cytokines and proteins which satisfy the metabolic needs of the non-vascularized tissues of the anterior eye segment. Among all of its components, it is important to remember sodium, potassium, chlorine, bicarbonate, glucose, urea, ureic acid, creatinine, enzymes such as cholinesterase, amylase, hyaluronidase, glycosidase and aldolase, as well as hyaluronic, ascorbic and lactic acids. The protein component is minimal, and it seems to derive from plasmatic filtration through fenestrated capillaries in the ciliary body[7, 10, 11].

Proteomic studies on AH or vitreous body, have become more common, in recent years, to investigate chorioretinal diseases[3]. The biodynamic of ocular fluids has demonstrated motion of molecules between the two compartments of the eye (vitreous cavity and anterior chamber). Moreover, some authors have demonstrated that the aqueous level of cytokines and chemokines reflect the vitreous one. The feasibility of AH sampling is therefore considered appropriate to study the pathophysiology of many chorioretinal disorders and also to evaluate any changes induced by different treatments[70].

2.4 OCULAR COMPLICATIONS DUE TO BRACHYTHERAPY

Conservative radiotherapy can affect almost every structure of the eye, resulting in several side effects that may require a specific management. In particular, Iodine-125 emits relatively low energy photons, which theoretically decrease radiation-related complications[71]. Despite this, this kind of brachytherapy is associated with complications, including: ocular surface and corneal alterations, cataract development,

chorioretinopathy, maculopathy and optic neuropathy diseases and neovascular glaucoma[71].

Dry eye was reported in 8.3% of patients and occurs about 20.7 months after treatment. Symptomatic treatment is recommended and includes topical lubricants[72]. Radiation is known to damage the lens equatorial fibres, due to their high mitotic rate, with the development of radiation cataract. The reported rate of cataract development after Iodine-125 brachytherapy for UM varies, from 8% to a predicted 83% by 5 years, as does the time to development, from 11 months to 35 months after treatment. With a cumulative dose to the lens of 24 Gy or more, the 5-year cumulative incidence of cataract was 92% compared with 65% in those with less than 12 Gy. The radiation dose to the lens is affected by both tumor size and location. Surgery (phacoemulsification with intraocular lens implantat) for radiation-induced cataracts is thus beneficial and safe for many patients, particularly in the short-term, although visual improvement is often limited by other, and less manageable, radiation complications[72].

A fearful complication due to eye irradiation is secondary glaucoma, with an incidence of between 3% to 56%. The primary risk factors associated with secondary glaucoma include: older age, larger tumor size, anterior location of the tumor, and higher baseline intraocular pressure (IOP). The first-line therapy for secondary glaucoma is IOP-lowering medical therapy which allows on most cases adequate control. Neovascular glaucoma, a form of secondary glaucoma, is the result of the neovascularization of the iris and the anterior chamber angle[72]. From a pathogenic perspective it is due to the release of proangiogenic factors from direct radiation damage to tumor endothelial cells. Additionally, secondary ischemic changes due to injury to the surrounding retinal tissue may contribute to the development of the iris neovascularization. Several parameters may contribute to the development or progression of neovascular glaucoma: tumor dimension, location, Bruch’s membrane rupture, associated serous retinal detachment. The reported incidence is of 8% at 50 months post-treatment. Neovascular glaucoma usually has a poor prognosis and may

lead to enucleation, thus early diagnosis and treatment is of essential importance. Medical therapy to control IOP, intravitreal injection and panretinal photocoagulation have been used in its treatment[72].
Side effects that deserve a separate chapter are those affecting the retina and the optic nerve[71, 72].

2.4.1 Radiation (Chorio)Retinopathy

Radiation retinopathy, better defined as radiation chorioretinopathy, is one of the major complications after eye irradiation. From a histopathological perspective characterized by progressive vascular remodeling, vascular occlusion and chorioretinal inflammation. This pathologic process is clinically characterized by the appearance of microaneurysms and telangiectasia and hard exudates from compromised retinal capillaries. Therefore, as the areas of capillary dropout become confluent, retinal ischemia develops with nerve fiber layer infarctions became visible (cotton wool spots). Usually, larger vessels are involved later in the course of the disease. When there are large or multiple areas of capillary non-perfusion, laser photocoagulation is mandatory to prevent retinal and disc neovascularization. Choroidal circulation is also directly compromised, thus suggesting that the term radiation chorioretinopathy better identifies this disorder[71, 73].

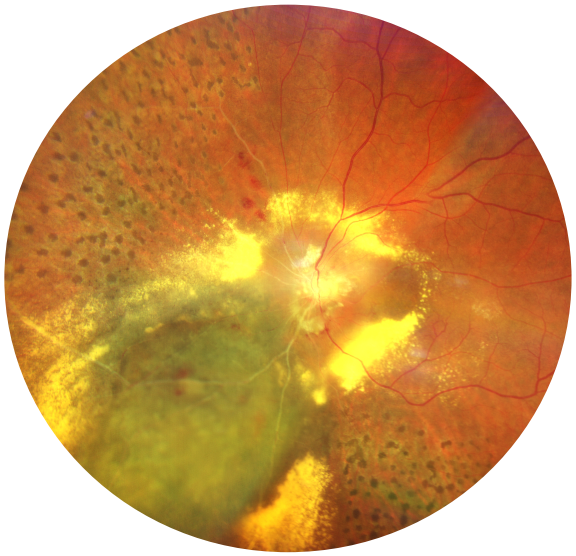

Figure 15. Color fundus photography showing a laser-treated radiation chorioretinopathy, characterized by chorioretinal atrophy, ischemia, ghost vessels, cotton wool spots, hard exudates and retinal hemorrhages; hemorrhages and hard exudates involve both the macular region (radiation maculopathy) and the optic nerve (radiation optic neuropathy).

2.4.2 Radiation Maculopathy

Radiation maculopathy describes the specific macular involvement secondary to eye irradiation. Its relevance is due to the peculiar role of the macula in the visual function. Its mean onset time is 20 months after irradiation, and it may cause significant and irreversible visual loss[71, 73]. Histopathologically, because of its high capillary density, macular microvasculature is more vulnerable to radiation damage. The pathologic process is clinically characterized by microaneurysms, telangiectasia, capillary non-perfusion, macular edema and hard exudates. Radiation maculopathy is clinically characterized by edematous changes in its early stages (cystoid macular edema) and/or by ischemia and atrophic changes in the macular area in more advanced stages. Moreover, an inflammatory component in its pathophysiology has been recently suggested, as well the presence of an “inflammatory phenotype”[71, 74, 75]. Actually, there are not defined guidelines for the treatment of radiation maculopathy and a clinical trial (protocol AL) is ongoing.

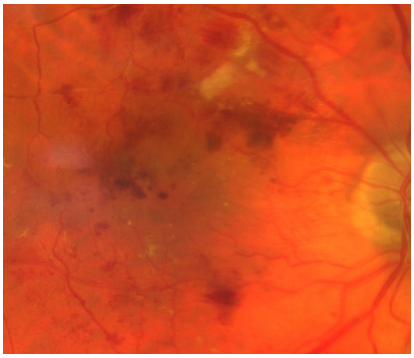

Figure 16: Color fundus photography showing radiation maculopathy characterized by both macular edema and ischemia,

cotton wool spots and retinal hemorrhages.

2.4.3 Radiation Optic Neuropathy

Radiation optic neuropathy is typically characterized by a rapid visual loss occurring months to years after optic nerve irradiation[71]. The main clinical findings include: hemorrhages and edema of the optic nerve head. Its pathogenesis includes primary radiation-induced axonal necrosis, vascular occlusion with subsequent axonal death or both[76]. The damage to the optic nerve is related to the total dose, tumor location and dimension and volume of optic nerve irradiated. It has already been shown that the anterior visual pathway does not tolerate cumulative doses greater than 50 Gy. The treatment for radiation optic neuropathy is still controversial, but the use of systemic corticosteroids and intravitreal injection are mainly used[72].

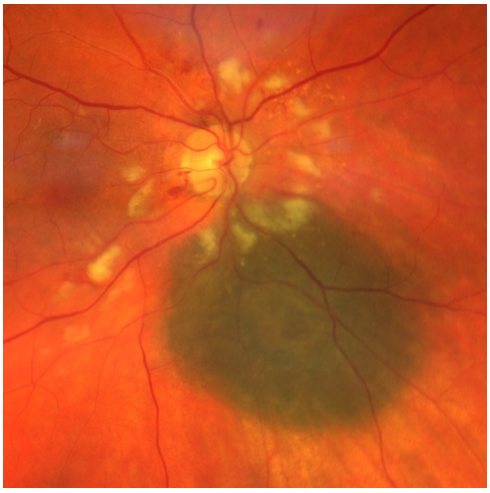

Figure 17: Color fundus image of radiation optic neuropathy.

2.5 OPTICAL COHERENCE TOMOGRAPHY

Figure 18. Image of SD-OCT HRA2+OCT (Heidelberg Engineering, Heidelberg, Germany).

Optical Coherence Tomography (OCT) is a non-invasive technique that allows to image retinal morphology at 5 μm resolution, producing cross-sectional and three-dimensional images of the central part of the retina. This technique is now well established in the diagnosis, management and treatment of almost all retinal and choroidal diseases, mainly to quantify the retinal thickness and to visualize the retinal pigment epithelium (RPE), neuroretina status and the choroid (using the specific enhanced depth imaging modality -EDI-). Spectral Domain OCT (SD OCT) uses a fixed reference mirror and a spectrometer which catches the incident signals. The information provided by the spectrometer is converted into the depth scans of the Fourier-transform[77]. Measuring thus all the light echoes simultaneously, the SD OCT increases significantly the quantity of data acquired with each scan, with a significant reduction in movement artifacts, an increase of signal-ground noise ratio, a greater image resolution, a more precise definition of retinal layers, a greater acquisition speed and a possibility to precisely map the optic nerve head. Moreover, SD OCT can elaborate 3D images and compare them to the photographic, angiographic and autofluorescence exams. OCT is normally used for the qualitative evaluation of the structural retinal pathologies caused by

several ocular diseases; therefore, it is necessary to obtain a segmentation of the different retinal layers[77, 78].

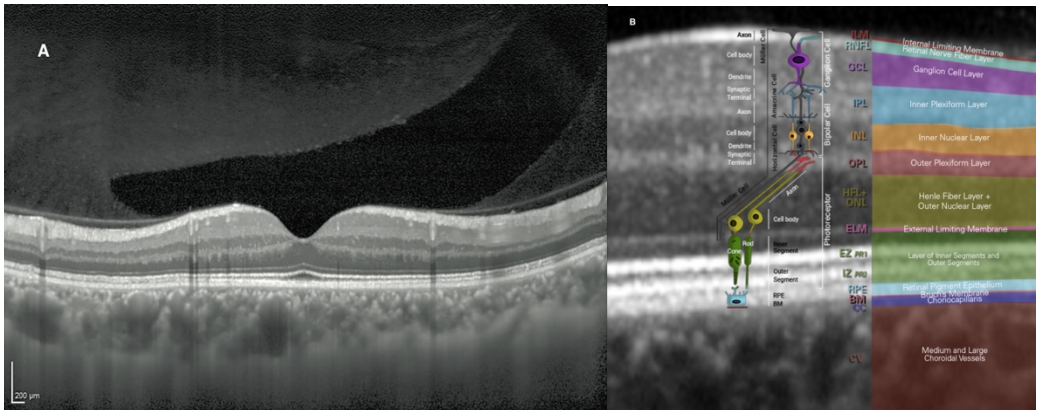

Figure 19. SD OCT image through the fovea (A) and corresponding nomenclature of retinal layers name and cells location (B).

2.5.1 Optical Coherence Tomography in Radiation Maculopathy

As already mentioned, OCT technique is now well established in the diagnosis, management and treatment of almost all retinal diseases, mainly to quantify the amount of macular edema, to visualize the RPE and to define the neuroretina status[71]. OCT is useful to identify and grade radiation macular edema, since its early stages, and correlate it with visual acuity[74, 79]. Recently, our group proposed a classification of radiation maculopathy using a multimodal imaging approach and a detailed multivariate statistical analysis: the cyst junction atrophy (CJA) classification, that can be used to clinically characterize and classify the disease stage as reported in Table 4[74].

Table 4. CJA Classification of Radiation Maculopathy

Features	Abbreviation	Grades	Grade Definition
Vertical size of the largest macular cyst *	C (cyst)	Cx	Vertical size of the largest macular cyst cannot be assessed †
		C_0	No evidence of measurable

			cysts;
		C_n	"n" indicates the vertical size of the largest macular cyst in μm ‡
IS/OS junction alterations *	J (IS/OS junction)	J_x	Presence of IS/OS junction alterations cannot be assessed †
		J_0	No evidence of IS/OS junction alterations
		J_1	Presence of IS/OS junction alterations
RPE atrophy *	A (RPE atrophy)	A_x	Presence of RPE atrophy cannot be assessed †
		A_0	No evidence of RPE atrophy
		A_1	Presence of RPE atrophy

IS/OS, photoreceptor inner segment/outer segment junction layer.

* Involving the central area (1 mm). † The use of this grade should be minimized. ‡ For example, in a patient having the vertical size of the largest macular cysts of 534 μm, the C grade is C534.

3. PURPOSE OF THE STUDY

There is growing interest in the field of ocular oncology, for the identification of diagnostic and prognostic biomarkers at ocular fluids level. Anterior chamber paracentesis is technically ordinary and safe procedure for the patient, so AH sampling and evaluation may represent the liquid biopsy approach in the diagnosis and follow-up of UM.

3.1 RESEARCH AIMS

- Evaluate the presence of AH neuroinflammatory, angiogenic and immune biomarkers in eyes affected by UM at the time of tumor treatment.
- Evaluate the presence of AH biomarkers strictly correlated with UM driver genes.

- Evaluate the changes of AH biomarkers after the conservative treatment for UM (I-125 brachytherapy).
- Evaluate the correlation between AH biomarkers and imaging biomarkers 20 months after the treatment for UM.

4. MATERIAL AND METHODS

4.1 STUDY POPULATION

Subjects planned for brachytherapy for primary UM underwent AH sampling during I-125 surgical procedure, before plaque positioning, whereas healthy subjects included in the control group, matched for age, underwent AH sampling at the time of cataract surgery. Moreover, immediately before plaque positioning Fine Needle Aspiration Biopsy (FNAB) procedure was performed in the UM group. Each subject underwent a complete ophthalmologic examination, including slit-lamp

biomicroscopy, ophthalmoscopy and OCT at baseline and during the follow-up. The location of the tumor was reported according to the main involved sector (nasal, temporal, superior, inferior) and the tumor origin (choroid, ciliary body). Tumor thickness and largest basal diameter, measured by A- and B-scan ultrasonography (Aviso, Quantel Medical, Clermont-Ferrand, France) were also reported. Tumors were staged using the 8th AJCC classification. The same UM subjects underwent AH sampling at the time of planned para surgical procedures 20 months after brachytherapy. Informed consent was obtained from each subject and Institutional Review Board approved the study protocol. The approval for the study was obtained from the local Ethics Committee (study N.:4828 Prot. N. 18682, February 20, 2020).

4.2 AQUEOUS HUMOR SAMPLE AND OMIC ANALYSIS

4.2.1 Collection and Conservation

Each subject underwent standard pre-operative preparation for eye surgery, including disinfection of periocular skin with povidone-iodine 10% (ESO- JOD, ECOLAB, Agrate Brianza, Italia), irrigation of the conjunctival sac with povidone- iodine 5% (Oftasteril, Alphaintes), abundant washing out of the eye with balanced salt solution. AH (150–200 µl/sample) was aspirated from the anterior chamber, using a 30-gauge needle connected to an insulin syringe (1 ml). After aspiration, AH was collected by a second operator in a single microfuge containing 10 µl of a cocktail of protease inhibitors (Pierce Biotechnology, Rockford, IL). Coded microvials were quickly stored at -80°C.

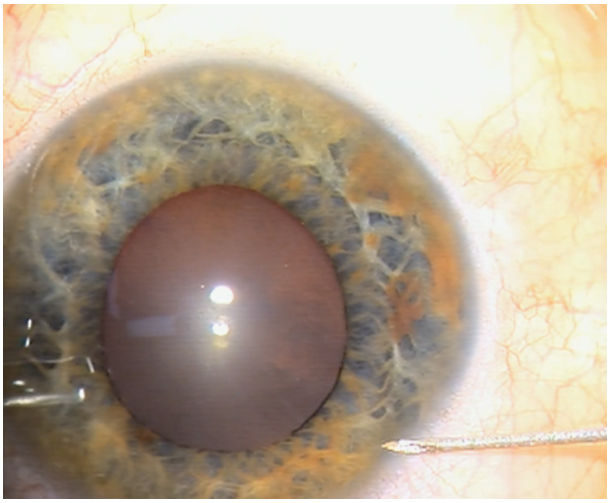

Figure 20. Aqueous humor sample collection.

4.2.2 Quantitative Determination of Total Proteins

The total protein content was quantified in 3μl/sample with a digital spectrophotometer (NanoDrop; Thermo Fisher Scientific Inc, Waltham, MA) and protein concentrations were calculated by means of the linearized standard curve (bovine serum albumin) using the A280 application. AH samples where than sonicated (VibraCell; Sonics, Newton, CT) and clear supernatants were provided by centrifugation (13,000 rpm/7 minutes).

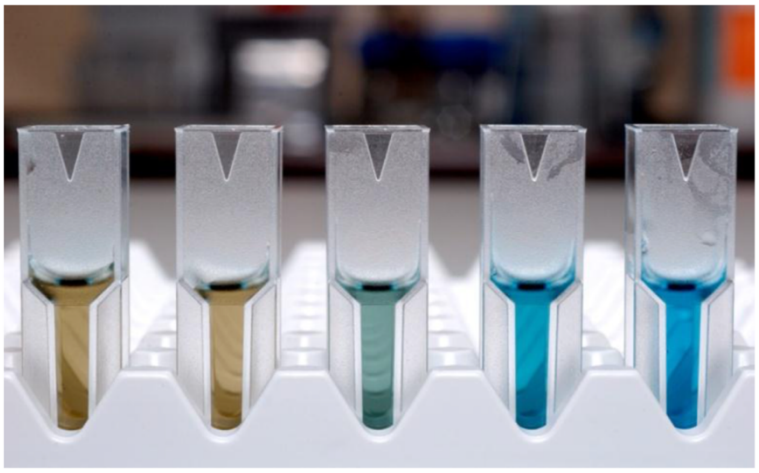

Figure 21. Protein quantification with Bradford method: from left to right we notice the increasing protein concentrations.

4.2.3 Protein Array

A customized protein array on glass-chips established by the manufacturer is used. Normalized and pre-diluted AH samples are loaded on chip arrays, according to the manufacturer's instruction, including target, positive, negative and internal control spots. After an overnight incubation at 4 °C, the array slides are washed and exposed to a biotinylated antibody mixture followed by a cy3-streptavidin labeling solution. All steps are performed under orbital shaking, with hybridization/washing solutions provided by the kit. Finally, glass-slides are washed, spin-dried and acquired with microarray scanner. To obtain appropriate Cy3/Cy5 (specific/background signals) images, the slides are scanned over previously validated acquisition parameters and procedures. The fluorescence signals are acquired with the microarray scanner. All comet tails are ignored and only median signal values obtained using the same setting are used for the identification of any biomarker variation. An inter- and intra–assay coefficient of variability limit of ≤10% was set for the study, and a 1.5-fold increase or ≤0.65-fold decrease in signal intensity is considered to guarantee specific signals above background. Fluorescent signals are analyzed and fold changes are generated.

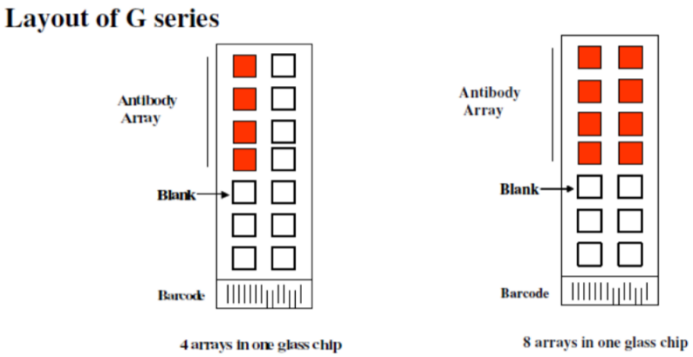

Figure 22. Protein array on glass-chip: the left one contains 4 chips, the right one 8 chips.

4.2.4 Immunoprecipitation, SDS PAGE and immunoblotting

Not-pooled samples were used for these studies. Targets were analyzed according to the direct immunoprecipitation (IP) technique coupled to Western Blotting analysis. The capture antibodies specific for GNAQ, BAP1, EIF1AX, SF3B1 and Inwardly rectifying potassium (Kir) 4.1 were pre-incubated with Pure Proteome Protein G Magnetic beads (15 µL, Millipore, Burlington, Massachusetts, USA) and immobilized with a magnet, to generate the antibody-beads complex. The beads-bound antibodies were then added to the normalized samples (30µg total protein/sample) and after 2 hrs incubation, the specific bounds were separated, washed and eluted in denaturing Loading Buffer. All steps were performed under orbital shaking (Certomat II, Sartorius AG). Loading Buffer and samples were preheated at 90°C for 10 min and loaded on 4%-12% precasted SDS-PAGE gels (Bio-Rad Laboratories Inc, Hercules, CA, USA) and electrophoresis was performed in a MiniProtean3 apparatus (Bio-Rad) under reducing conditions (120 V/frontline). Electrophoresed bands were transferred to 0.22µm membranes (Hybond, GE Healthcare, Buckinghamshire, UK) at 12 V/40 min in a semidry Trans-Blotting apparatus (Bio-Rad). Membranes were stained with the high-sensible Sy-pro Ruby protein blot stainer to verify the presence of specific bands (Invitrogen, Waltham, Massachusetts, USA), ac-cording to a standard procedure. Immunoblotting with specific detection antibodies and chemiluminescent developing were performed to visualize and acquire the target of interest. The analysis of intensity density (IntDen) was performed for each band, using the free available ImageJ software (Image J v1.43; NIH http://rsb.info.nih.gov/ij/). Images were saved as 8-bit TIFF files and data (IntDen) were exported for figure assembly using the Adobe Photoshop (2022) 22.0.0 software (Adobe Systems Inc., San Jose, CA).

4.2.5 Enzyme-Linked Immunosorbent Assay

Glial fibrillary acidic protein (GFAP) and aquaporin 4 (AQP4) levels were quantified using commercial high-sensitive enzyme-linked immunosorbent assays (ELISA), according to the manufacturer's suggestions with minor

modifications. Briefly, prediluted samples and standard curve were diluted in TBS buffer (20 mM Tris-Cl and 150 mM NaCl; pH 7.5) containing 3% bovine serum albumin, 5 mM EDTA, and 1X protease inhibitor cocktail, and loaded on 96-well precoated plates. Biotin-coupled antibodies and horseradish peroxidase-streptavidin–specific bindings were used and specific binding was developed with a ready-to-use tetramethylbenzidine substrate (eBioscience, San Diego, CA). The colorimetric signal was quantified using an enzyme- linked immunosorbent assay reader at 490 to 560 mm (Sunrise; Tecan Group Ltd, Männedorf, Switzerland). The optical density (OD) data were normalized to total protein content (NanoDrop). The specific GFAP and AQP4 concentrations were calculated on the linearized standard curves, as provided at the end of enzyme-linked immunosorbent assay.

4.3 FINE NEEDLE ASPIRATION BIOPSY

Fine Needle Aspiration Biopsy (FNAB) procedure was performed using a 25-gauge spinal needle connected to a 10 cc syringe by a hollow tube. The needle was inserted into the tumor through a 300μm scleral incision (to avoid excessive pressure when penetrating the eye). A double-pass sampling was performed. The scleral incision was sutured and the radioactive plaque immediately placed over the tumor base. Tumor specimens obtained by FNAB were collected in culture medium RPMI 1640 (Euroclone Life Science, Pero-MI, Italy).

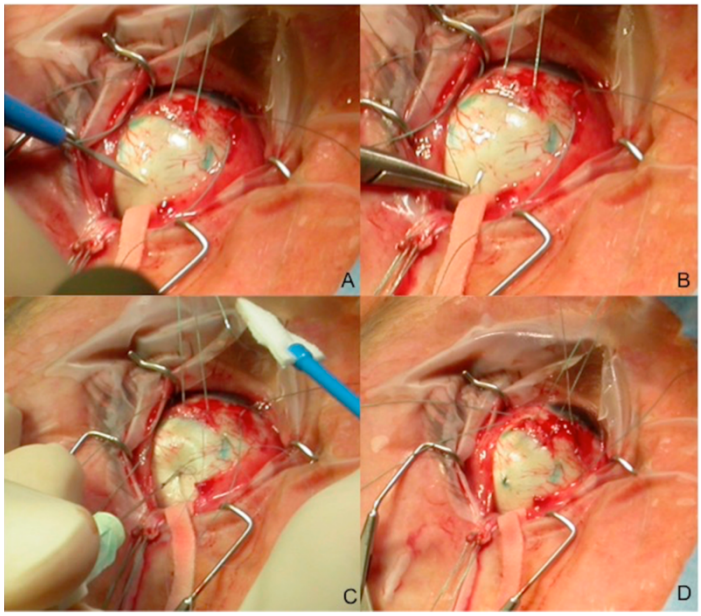

Figure 23. Fine Needle Aspiration Biopsy (FNAB) sample: transscleral approach in a posterior uveal melanoma. Our standard FNAB procedure is performed using 25 gauge (25mm in length) spinal needle connected to a 10cc syringe by a hollow tube. (A) The needle is inserted into the tumor trough a partial scleral incision (to avoid excessive pressure when penetrating the eye). (B) The scleral suture (7.0 Polyglactin) is prepared before the needle insertion. (C) A double-pass sampling is performed through the same scleral access. (D) The scleral incision is then sutured and the radioactive plaque immediately placed over the tumor base.

4.3.1 Cytogenetic Analysis

The sampled material underwent fluorescence in situ hybridization (FISH). After sedimentation, the material was enzymatically digested with collagenase II (Worthington, NJ. USA) 1400 U/mL at 37 °C for 2 hours. Then the suspension was washed in RPMI 1640 and used to prepared cytospins. Slides were fixed with a cytologic fixative (Bio- Fix; Bio-Optica, Milano, Italy), and stored at –20 °C. FISH analysis was performed with a centromeric probe for chromosome 3 labeled with SpectrumOrange and centromeric probe for chromosome 10 labeled with SpectrumGreen (Abbott-Vysis, Downers Grove, IL, USA) following the manufacturer's procedure. Slide and probe were codenatured in Hybrite' (Vysis) at 75 °C

for 5’ and hybridized in a humid chamber overnight at 42 °C. Post-hybridization washes were made at 73 °C in 0.4 x SSC/0.3% NP-40 for 2’ and at room temperature in 2 x SSC/0, 1% NP-40 for 1’. Slides were air dried and mounted with a Vectashield, mounting medium with DAPI (Vector Laboratories, Burlingame). Microscope analysis was carried out with a fluorescent microscope (Zeiss Axioplan fluorescent microscope, Germany) equipped with a cooled charge-coupled device (CCD) camera (Hamamatsu, Hamamatsu-city, Japan) and appropriate single band and triple band filters. Images were analyzed using CRO- MOFISH software (Amplimedical, Assago-MI, Italy). At least 100 cells were evaluated for each case; loss of chromo-some 3 was reported when more than 15% of cells showed a single signal for chromosome 3.

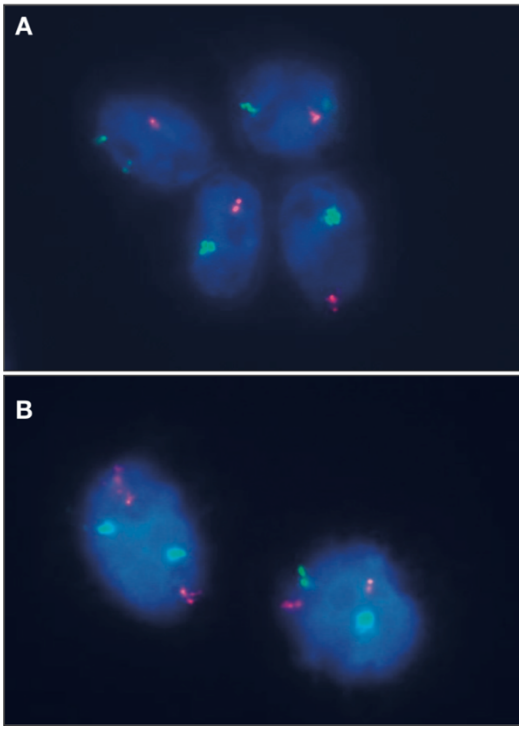

Figure 24. Fluorescence in situ hybridization analysis of tumor material sampled by fine needle aspiration biopsy. (A) A case with monosomy 3: each cell has two chromosomes 10 (labeled in green as controls), but only one chromosome 3 (labeled in red). (B) A case with disomy 3: each cell has two chromosomes 3 (in red) and two chromosomes 10 (in green).

4.4 OPTICAL COHERENCE TOMOGRAPHY ANALYSIS

Radiation macular edema (RME) was defined as the occurrence of macular thickening involving the center of the fovea and secondary to eye irradiation. All eyes underwent full ophthalmic examination including standard digital color fundus photography (Clarus 500; Carl Zeiss Meditec AG, Jena, Germany) and OCT. OCT scans were acquired using Spectralis HRA+OCT2 (Heidelberg Engineering, Heidelberg, Germany). In each eye, a map centered on the macula using en face OCT was performed. Spectral domain OCT scans in this study were obtained covering a 6.0 x 6.0 mm area centered on the macula and consisting of 97 horizontal B-scan lines with 512 A-scans per line. B-scans were obtained at an interval of 60 mm between lines. Moreover, the clinical evaluation of OCT scans assessed the presence of intra- and sub-retinal fluid and disruption of both external limiting membrane ad ellipsoid zone. After segmentation of retinal layers, a 3000 μm area focused on the fovea was defined by two vertical lines allowing to analyze the selected central OCT linear scan at 180°. The en face imaging also granted a precise location of hyperreflective retinal foci (HRF). Hyperreflective retinal foci were evaluated on the central B scan passing through the fovea, which was displayed on a monitor simultaneously with and below an en face map. Hyperreflective retinal foci were defined as discrete intraretinal reflectivity changes < 30 μm, characterized by reflectivity similar to the nerve fiber layer and the absence of back shadowing. Hyperreflective retinal foci were analyzed within the a 3000 μm foveal area and characterized in the inner retina from the ganglion cell layer to the inner nuclear layer and in the outer retina from the outer plexiform layer to the outer nuclear layer.

4.5 STATISTICAL ANALYSIS

Data are presented as the mean ± standard deviation, and the normality of the distribution was assessed by the Shapiro–Wilk test. The comparison of AH proteins' expression in patients with UM and in controls was made, for each protein, by means of Wilcoxon-Mann-Whitney test with Bonferroni

correction of a post hoc significance level. Linear regression was applied to see whether clinical and genetic characteristics correlated with each protein level. Protein expression cut-off values were investigated. Area under ROC curve was computed and its significance was tested by Mann–Whitney test. Cut-off values were identified according to various criteria (distance to corner, sensitivity-specificity difference and Youden index). Graduation of protein expression in UM group was performed through quartiles of the sampling distribution. Hierarchical cluster analysis (agglomerative procedure) was used to organize proteins and cases, respectively, and Wilcox-on-Mann-Whitney was applied to compare the clusters. The comparisons between subjects with and without RME were made by means of Wilcoxon–Mann–Whitney test for independent samples. A value of $p < 0.05$ was considered statistically significant. Linear regression was applied to see whether imaging (OCT) features correlated with proteins level. Data were analyzed using SAS statistical software (SAS 9.2; SAS Institute, Cary, NC, USA).

5. RESULTS

5.1 Population

Seventy-two subjects with UM (72 eyes) and 36 controls (36 eyes) were included. The mean age at study inclusion was 59.32±11.78 and 61.81±5.42, respectively for cases and controls (p=0.312). The mean age at study inclusion was 67.5±12.5 and 62.7±18.4, respectively for cases and controls (p=0.321). There was no significant difference in gender (p=0.225) between the two study groups. In the UM group, sixty patients (83%) were affected by only choroidal tumor and twelve patients (17%) by choroid and ciliary body tumor. According to the AJCC 8th classification, tumor size categories were T4 in 18 eyes (25%), T3 in 34 eyes (47%) and T2 in 20 eyes (28%). The mean tumor thickness was 8.6±3.6 mm and largest basal diameter 16.1±2.4 mm. No complications after AH sampling and FNAB were reported in both groups. Transscleral FNAB yielded enough material for FISH analysis in all the 72 cases (100%). Monosomy 3 was detected in 34 cases (47%) and disomy 3 in 38 cases (53%). Among the monosomy 3 tumors, the mean percentage of monosomic cells in each sample was 90% ± 9.3% (range, 74-100%).

5.2 Inflammatory Proteins and Uveal Melanoma

Compared with the control group, as shown in Figure 25, significantly higher levels of SSTR1 (p=0.028), HMB45 (p=0.018), IL-6 (p=0.047), IL-8 (p=0.008), RANTES (p=0.008), PEDF (p=0.048), Osteopontin (p=0.048), EGF (p=0.041), bFGF (p=0.019), MIF (p=0.009), MCP-1 (p=0.023) were detected in eyes with UM. VEGF concentration difference between the two groups was statistically borderline (p=0.055).

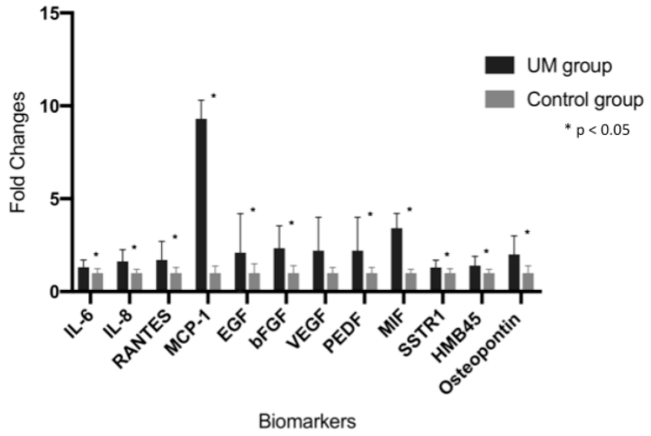

Figure 25. Representation of fold changes ± SD of each AH dosed biomarker in uveal melanoma eyes (UM group) versus control eyes (control group).

* = proteins showing a statistically significant difference ($p<0.05$) between study and control group. VEGF concentration showed a borderline difference ($p=0.055$).

Compared to UM with disomy 3, significant higher levels of IL-6 ($p=0.022$) IL-8 ($p=0.003$), RANTES ($p=0.005$), EGF ($p=0.018$), bFGF ($p=0.012$), VEGF ($p=0.026$), MIF ($p=0.005$) and MCP-1 ($p=0.005$) were detected in UM with monosomy 3, as shown in Figure 26.

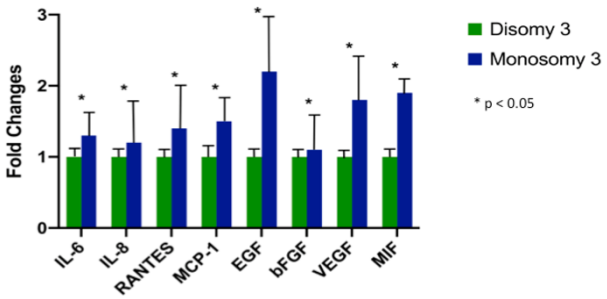

Figure 26. Representation of fold changes ± SD of each AH protein in uveal melanoma with monosomy 3 versus uveal melanoma without monosomy 3.

* = proteins showing a statistically significant difference ($p<0.05$) between study and control group.

Comparison between monosomy 3 UM with clinical characteristics and cytokine concentrations showed a positive correlation between: tumor thickness and IL-8 (p=0.022), tumor thickness and VEGF (p=0.031), LBD and RANTES (p=0.015), and degree of retinal detachment and IL-6 (p=0.021).

5.3 Prognostic Proteins: GNAQ, BAP1, SF3B1, EIF1AX

GNAQ, BAP1, SFT3B1 and EIF1AX levels in the AH samples are shown in Figure 27. Compared to the control group, significant higher levels of GNAQ (p=0.022), BAP1 (p=0.013) and SF3B1 (p=0.023) were detected in eyes with UM.

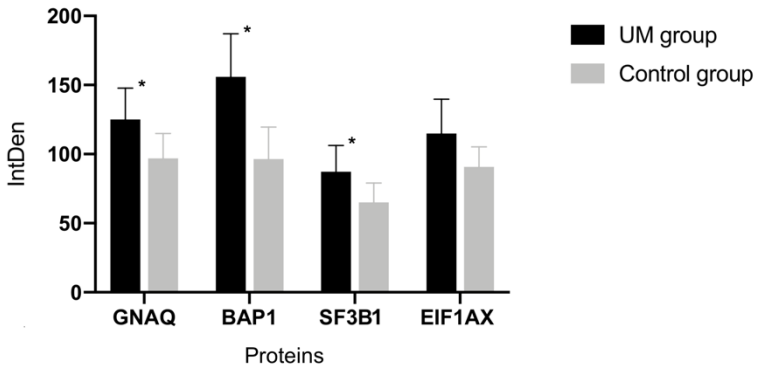

Figure 27. Representation of immunoprecipitation and SDS PAGE analysis of aqueous humor dosed proteins in uveal melanoma eyes (UM group) versus cataract eyes (control group). Expression levels (integrated density values) are given in arbitrary units.
* = proteins showing a statistically significant difference ($p<0.05$) between study and control group.
IntDen: integrated density.

No statistically significant correlations between clinical features (age, LBD, tumor height, tumor stage) and proteins expression were observed. Moreover, no statistically significant correlations between GNAQ, BAP1, SF3B1 and EIF1AX protein expression and chromosome 3 status were

reported. Furthermore, mean values of proteins expression were also analyzed in order to find cut-off values to identify different classes of protein expression, as shown in Table 5.

Table 5. Cut-off values of protein expression in uveal melanoma

	Expression Levels		
Proteins	**Low**	**Medium**	**High**
GNAQ	<112.8	112.8-145.5	>145.5
BAP1	<128.4	128.4-182.2	>182.2
EIF1AX	<86.8	86.8-135.7	>135.7
SF3B1	<81.9	81.9-93.3	>93.3

The protein expression levels for each UM subject were recorded and expressed with the information regarding chromosome 3 status, as shown in Figure 28.

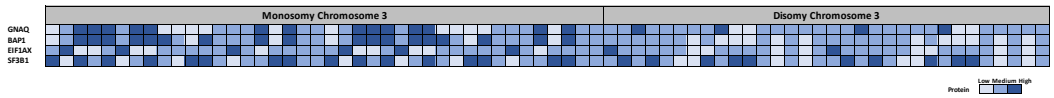

Figure 28. Heatmap showing expression of GNAQ, BAP1, EIF1AX and SF3B1 for each UM subject, divided according to chromosome 3 status.

Furthermore, cluster analysis of UM group revealed two clusters. In particular, one consisting of 30 cases showing higher expression of GNAQ and BAP1 and low presence of EIF1AX; another consisting of 42 cases with higher expression of EIF1AX and lower expression of GNAQ and BAP1, as shown in Figure 29.

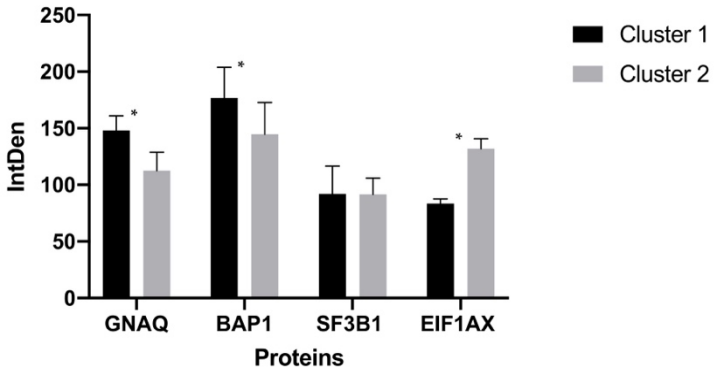

Figure 29. Representation of immunoprecipitation and SDS PAGE analysis of aqueous humor proteins dosed by clusters. Expression levels (integrated density values) are given in arbitrary units. Data are shown as mean ± SD.

* = proteins showing a statistically significant difference ($p<0.05$) between clusters.

IntDen: integrated density.

The two clusters differed significantly in monosomy and disomy ($p=0.021$) of chromosome 3, with the cluster with more expression of GNAQ and BAP1 showing monosomy 3. Furthermore, the protein expression levels for each UM subject were recorded and expressed with the information regarding cluster, as shown in Figure 30.

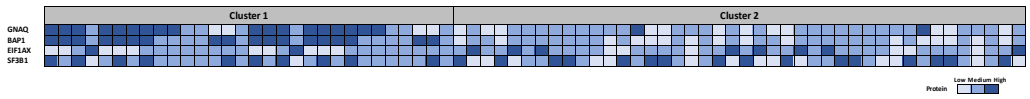

Figure 30. Heatmap showing expression of GNAQ, BAP1, EIF1AX and SF3B1 for each UM subject, divided according to cluster.

5.4 Omic and Imaging in Radiation Maculopathy

Finally, the AH of the UM group 20 months after the treatment showed that 22 subjects (30.5%) developed RME. All RME eyes at OCT analysis had significant increase in thickness of inner and middle retinal layers ($p=0.035$) mostly determined by intraretinal fluids ($p=0.002$), in number of

hyperreflective retinal foci (p=0.023) and in areas of disrupted external limiting membrane (p=0.014) as shown in Table 6.

Table 6. Radiation maculopathy imaging features

OCT Features	UM group with RME	UM group without RME	p value
CST (µm)	550±35	229±30	**0.035**
IRF (%)	95	0	**0.002**
SRF (%)	60	0	0.051
HRF (n°)	87±6.7	30±5.2	**0.023**
Disrupted ELM (%)	25	0	**0.014**
Disrupted EZ (%)	16	0	0.064

CST: central subfield thickness; IRF: intraretinal fluid; SRF: subretinal fluid; ELM: external limiting membrane; EZ: ellipsoid zone.

GFAP, Kir 4.1 and all inflammatory biomarkers were dramatically increased in RME eyes compared to those without RME (p=0.035, p=0.021 and p=0.032 respectively), as shown in Figure 31.

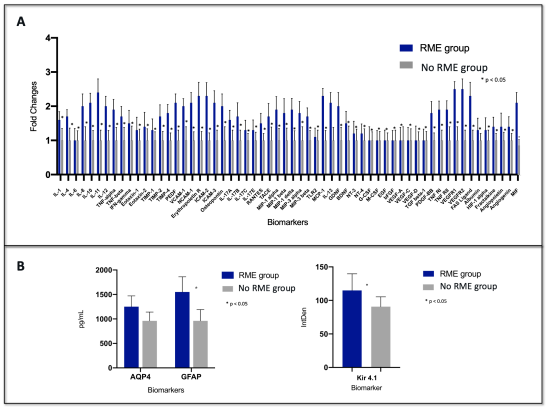

Figure 31. Representation of protein array (A), ELISA (AQP4 and GFAP) and immunoprecipitation- SDS PAGE analysis (Kir 4.1) (B) of selected aqueous humor proteins. Data are shown as mean ± SD.

* = proteins showing a statistically significant difference (p<0.05) between clusters.

IntDen: integrated density.

Finally, a statistically significant direct correlation between intraretinal fluid and HRF was found for both inflammatory biomarkers and Kir 4.1 (p=0.025) as shown in Figure 32.

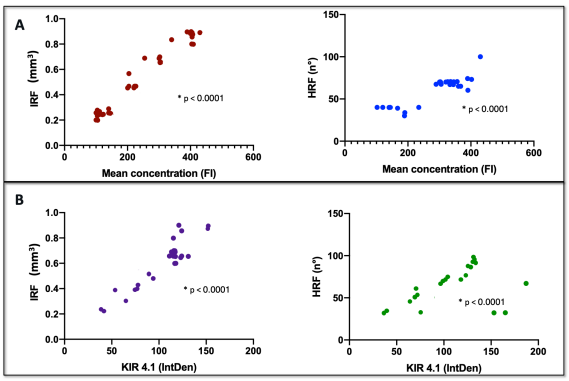

Figure 32. Correlation between inflammatory biomarkers and intraretinal fluid and hyperreflective foci (A) and between Kir 4.1 and intraretinal fluid and hyperreflective foci. IRF: intraretinal fluid; HRF: hyperreflective retinal foci.

6. DISCUSSION AND CONCLUSIONS

Several clinical, histopathological and genetic markers have been identified to define UM features and prognosis[23]. Classically, the TNM staging, the cell type (epithelioid cells) and the chromosome 3 status (monosomy 3) have been identified as unfavorable prognostic factors[23, 80]. Currently, it has been established that the tumor microenvironment and tumor genetic characteristics play a leading role in UM. The tumor microenvironment is the environment surrounding the tumor, and it includes: extracellular matrix, blood vessels, inflammatory/immune cells and signaling molecules[29, 81]. The tumor is closely related to the microenvironment and therefore the last one reflects the nature of the tumor itself. It is reported also for UM that the inflammatory/immune cells infiltration is related to the prognosis. The inflammatory phenotype of UM, characterized by high infiltration of lymphocytes and macrophages is associated to a poor outcome. Moreover, recent findings reported that the microenvironment influences the expression of inhibitory immune checkpoints[29, 81, 82].

The identification of proteins in intraocular fluids has recently assumed great relevance in the pathophysiological characterization of different retinal and choroidal diseases[3, 70]. The peculiar correlation between the concentration of proteins in the vitreous and those in the AH has already been reported, confirming the value of aqueous sampling as a less invasive procedure compared to the vitreous one. Since the identification of aqueous flare in UM eyes, the relevance of soluble factors interactions in UM microenvironment has been suggested[70, 83].

In our cohort, we have found a significantly higher concentration of inflammatory factors such as IL-8, IL-6, RANTES and MCP in UM eyes[23, 59, 80, 84-87]. A significant increase of some pro-inflammatory molecules (mainly IL-8, RANTES and MCP) has already been reported by Usui et al who compared eyes affected by UM to eyes affected by benign choroidal nevi[57]. Conversely, the same Authors didn't find increased IL-6 levels, as we did[57]. IL-6 is a well-known pro-inflammatory cytokine, typically

produced by T lymphocytes and macrophages, implicated in the persistence of the inflammatory cycle[57]. Our results showed a slightly significant increase of IL-6 in UM eyes compared to controls, but a statistically significant increase of this cytokine in monosomy 3. Recently, Gezgin et al demonstrated on histopathologic samples, that monosomy 3 correlates with an increased influx of T cells[88]. Probably this T cell infiltration in UM may cause the secretion of IL-6 and its higher concentration. Moreover, a stronger correlation between serous retinal detachment amount and IL-6 was found, suggesting that IL-6 secretion may be also related to the serous retinal detachment that clinically characterized UM[86]. Furthermore, our data confirmed the relevance of IL-8 and MCP-1 in UM. These molecules are chemotactic factors, involved in the recruitment of TAM into tissues, and facilitating the proliferation and survival of UM[89]. Furthermore, our data showed that RANTES positively correlated with largest basal diameter in UM with monosomy 3.

Moreover, we found a higher concentration of MIF in UM eyes, especially in monosomy 3. MIF is a pleiotropic cytokine normally present in the AH, which inhibits natural killer (NK)-cells, thus protecting malignant cells from their surveillance[86]. Several ocular tissues produce MIF, and Repp et al already proved that human UM derived cells constitutively produce MIF[59]. Moreover, they observed that MIF expression was highest in monosomy 3 and UM metastasis derived cells.

Concerning the recent genetic landscape, mutations in GNAQ are frequently observed in primary UM. BAP1 and SF3B1 mutations are found most frequently in metastatic disease, whereas EIF1AX gene mutation is related to a favorable prognosis[23, 29, 30, 90, 91]. In our cohort, we have found in AH a significantly higher concentration of GNAQ protein in the UM group compared to control, therefore its overexpression in AH may reflect the hyperactive state of the protein in the tumoral tissue, which is essential for activating the tumor growth. Fortunately, even if GNAQ is essential to promote tumorigenesis, it is insufficient to induce the complete malignant transformation and in particular the aggressiveness of UM is

determined by secondary driver mutations[92]. Unexpectedly, the significant difference in GNAQ protein levels between cluster 1 and 2 may be due to the fact that GNAQ is the most common driver mutation, but not the only one. Therefore, in cluster 2 UM own probably a greater variability in driver alterations, which are usually mutually exclusive[23]. Regarding BAP1, our data demonstrated the overexpression of BAP1 in AH in the UM group and this may reflect the increased cytoplasmic localization of the protein[90, 93-97]. Moreover, this finding is consistent with Smit et al that stated how some BAP1-mutated/immunohistochemically BAP1-negative UM still show expression of BAP1, suggesting that negative nuclear staining for BAP1 may be due to an unexplained different mechanism[29]. Mutations in SF3B1 have been seen in advanced chronic lymphocytic leukemia, myelodysplastic syndromes and breast cancer. In our cohort, we have found, in AH, a significantly higher concentration of SF3B1[98]. EIF1AX mutations have been reported in several tumors and these mutations are assumed to result in increased or altered protein function[92]. Mutations have been recurrently seen associated to cases of UM without monosomy 3 analysis. This is consistent with the results of our clustering analysis, in which cluster 2 showed EIF1AX hyperexpression and a statistically significant association with disomy 3. Therefore, these data confirmed that EIF1AX-mutant tumors showed a low-risk form of the disease.

Furthermore, although radiotherapy still represents the gold standard for the conservative treatment of UM, radiation maculopathy is still a serious and poorly predictable adverse effect[71, 72]. The complex pathophysiology of radiation maculopathy cannot be fully explained by the sole vascular involvement. Therefore, it has been hypothesized that its pathogenesis may also include an “inflammatory pathway” that can be described because of the “cell senescence phenomenon”[71, 75]. Therefore, our study combining both imaging and proteomic biomarkers, assessed the role of neuroinflammation in the pathophysiology or radiation maculopathy. In particular, HRF have been proposed as activated and

aggregated microglial cells, representing an *in vivo* marker of local inflammatory response[79, 99-102]. Furthermore, we found a significant increase in GFAP and Kir 4.1 expression in subjects with radiation maculopathy; these proteins are produced by Müller cells, which are normally activated during the development of macular edema[103, 104]. Usually, GFAP is mostly expressed in the normal retina by astrocytes. Nevertheless, in the pathogenesis of macular edema, it has been well established that Müller cells are activated early and one of the most prominent signs of Müller cell activation is the (increased) expression of GFAP, whereas astrocytes undergo a precocious cell death by apoptosis[103, 105]. Müller cells produce factors capable of modulating blood flow, vascular permeability, cell survival, and neuroprotection, besides extra and intracellular water transport[103, 105, 106]. Therefore, injury to these cells has an essential role in the pathogenesis of early microcirculatory abnormalities and neurodegeneration, as shown in several kinds of macular edema, in particular the one related to diabetes[13, 15, 16]. The same protein increase was found for Kir 4.1. This transmembrane protein belongs to a large family of K+ channels and is the principal mammalian subunit expressed in Müller cells, regulating K+ conductance and strongly influencing simultaneous water transport across the cellular membrane. As already demonstrated in several retinopathies, Müller cells activation promotes additional localization of Kir 4.1 toward the apical microvilli of the cells. Therefore, the impaired expression and altered localization of Kir 4.1 cause a loss of function of the channel, with consequent K+ currents reduction and liquid accumulation (with the appearance of macular edema)[13, 103, 105]. These results offer fully new insights about the pathophysiology of radiation macular edema. Neuroinflammation secondary to the radiation-induced senescence mechanism of the primary tumor (typical reaction following irradiation of solid tumors) is probably one of the most relevant causes of radiation macular edema[71, 74, 75]. These data strongly support the hypothesis

that radiation macular edema is a retinal neuroinflammatory disorder and the current therapeutic approach needs to be revisited.

Finally, the whole study not only confirm *in vivo* the possibilities offered by AH analysis in UM eyes, but confirm that AH evaluation may represent the liquid biopsy approach in UM diagnosis, prognosis and follow-up.

7. BIBLIOGRAPHY

1. Tsimberidou, A.M., et al., *Review of precision cancer medicine: Evolution of the treatment paradigm.* Cancer Treat Rev, 2020. **86**: p. 102019.
2. Konig, I.R., et al., *What is precision medicine?* Eur Respir J, 2017. **50**(4).
3. Midena, E., et al., *Intraocular fluid biomarkers (liquid biopsy) in human diabetic retinopathy.* Graefes Arch Clin Exp Ophthalmol, 2021. **259**(12): p. 3549-3560.
4. Chang, A., et al., *Retina Update: Entering an Era of Personalized Medicine in Ophthalmology.* Asia Pac J Ophthalmol (Phila), 2023. **12**(2): p. 111-112.
5. Lauwen, S., et al., *Omics Biomarkers in Ophthalmology.* Invest Ophthalmol Vis Sci, 2017. **58**(6): p. BIO88-BIO98.
6. Kwan, C.C. and A.A. Fawzi, *Imaging and Biomarkers in Diabetic Macular Edema and Diabetic Retinopathy.* Curr Diab Rep, 2019. **19**(10): p. 95.
7. Anastasi G, C.S., Carnazza ML, Cinti S, De Caro R, Donato RF, Ferrario VF, Fonzi L, Franzi AT, Gaudio E, Geremia R, Giordano Lanza G, Grossi CE, Manzoli FA, Mazzotti G, Michetti F, Miscia S, Mitolo V, Montella A, Oriandini G, Paparelli A, Renda T, Ribatti D, Ruggeri A, Sirigu P, Soscia A, Tredici G, Vitale M, Zaccheo D, Zauli G, Zecchi S., *Apparato della vista. In: Trattato di Anatomia Umana*. 2007: Edi-Ermes.
8. E, M., *Anatomia. In: Malattie dell'apparato visivo*. 2006, Cedam.
9. Carol L. Shields, J.A.S., *Intraocular Tumors: An Atlas and Textbook*, ed. L.W.a. Wilkins. 2015.
10. Denniston, A., Murray, P, *Oxford Handbook of Ophthalmology, 4th edition*. Oxford University Press. 2018.
11. Leonard A Levin, S.F.E.N., James Ver Hoeve, Samuel Wu, Paul L. Kaufman, Albert Alm, *Adler's Physiology of the Eye*. 2011.
12. Xie, R., et al., *Evaluation of Choroidal Thickness Using Optical Coherent Tomography: A Review.* Front Med (Lausanne), 2021. **8**: p. 783519.
13. Reichenbach, A. and A. Bringmann, *Glia of the human retina.* Glia, 2020. **68**(4): p. 768-796.
14. Vecino, E., et al., *Glia-neuron interactions in the mammalian retina.* Prog Retin Eye Res, 2016. **51**: p. 1-40.
15. Coorey, N.J., et al., *The role of glia in retinal vascular disease.* Clin Exp Optom, 2012. **95**(3): p. 266-81.
16. Carpi-Santos, R., et al., *Contribution of Muller Cells in the Diabetic Retinopathy Development: Focus on Oxidative Stress and Inflammation.* Antioxidants (Basel), 2022. **11**(4).
17. Reichenbach, A. and A. Bringmann, *New functions of Muller cells.* Glia, 2013. **61**(5): p. 651-78.

18. Zhan, J.S., et al., *Astrocytes in Migration.* Neurochem Res, 2017. **42**(1): p. 272-282.
19. Silverman, S.M. and W.T. Wong, *Microglia in the Retina: Roles in Development, Maturity, and Disease.* Annu Rev Vis Sci, 2018. **4**: p. 45-77.
20. Fan, W., et al., *Retinal microglia: Functions and diseases.* Immunology, 2022. **166**(3): p. 268-286.
21. Altmann, C. and M.H.H. Schmidt, *The Role of Microglia in Diabetic Retinopathy: Inflammation, Microvasculature Defects and Neurodegeneration.* Int J Mol Sci, 2018. **19**(1).
22. Wang, S.K. and C.L. Cepko, *Targeting Microglia to Treat Degenerative Eye Diseases.* Front Immunol, 2022. **13**: p. 843558.
23. Jager, M.J., et al., *Uveal melanoma.* Nat Rev Dis Primers, 2020. **6**(1): p. 24.
24. Singh, A.D. and T. Kivela, *The collaborative ocular melanoma study.* Ophthalmol Clin North Am, 2005. **18**(1): p. 129-42, ix.
25. Branisteanu, D.C., et al., *Uveal melanoma diagnosis and current treatment options (Review).* Exp Ther Med, 2021. **22**(6): p. 1428.
26. Kujala, E., T. Makitie, and T. Kivela, *Very long-term prognosis of patients with malignant uveal melanoma.* Invest Ophthalmol Vis Sci, 2003. **44**(11): p. 4651-9.
27. Kaliki, S., C.L. Shields, and J.A. Shields, *Uveal melanoma: estimating prognosis.* Indian J Ophthalmol, 2015. **63**(2): p. 93-102.
28. Carvajal, R.D., et al., *Metastatic disease from uveal melanoma: treatment options and future prospects.* Br J Ophthalmol, 2017. **101**(1): p. 38-44.
29. Smit, K.N., et al., *Uveal melanoma: Towards a molecular understanding.* Prog Retin Eye Res, 2020. **75**: p. 100800.
30. Field, M.G., et al., *Punctuated evolution of canonical genomic aberrations in uveal melanoma.* Nat Commun, 2018. **9**(1): p. 116.
31. Kivela, T., *Diagnosis of uveal melanoma.* Dev Ophthalmol, 2012. **49**: p. 1-15.
32. Chattopadhyay, C., et al., *Uveal melanoma: From diagnosis to treatment and the science in between.* Cancer, 2016. **122**(15): p. 2299-312.
33. Solnik, M., et al., *Imaging of Uveal Melanoma-Current Standard and Methods in Development.* Cancers (Basel), 2022. **14**(13).
34. Amin, M.B., et al., *The Eighth Edition AJCC Cancer Staging Manual: Continuing to build a bridge from a population-based to a more "personalized" approach to cancer staging.* CA Cancer J Clin, 2017. **67**(2): p. 93-99.
35. Zimmerman, L.E., I.W. McLean, and W.D. Foster, *Does enucleation of the eye containing a malignant melanoma prevent or accelerate the dissemination of tumour cells.* Br J Ophthalmol, 1978. **62**(6): p. 420-5.
36. Singh, A.D., et al., *The Zimmerman-McLean-Foster hypothesis: 25 years later.* Br J Ophthalmol, 2004. **88**(7): p. 962-7.

37. Nathan, P., et al., *Overall Survival Benefit with Tebentafusp in Metastatic Uveal Melanoma.* N Engl J Med, 2021. **385**(13): p. 1196-1206.
38. Diener-West, M., et al., *The COMS randomized trial of iodine 125 brachytherapy for choroidal melanoma, III: initial mortality findings. COMS Report No. 18.* Arch Ophthalmol, 2001. **119**(7): p. 969-82.
39. Frizziero, L., et al., *Uveal Melanoma Biopsy: A Review.* Cancers (Basel), 2019. **11**(8).
40. *Histopathologic characteristics of uveal melanomas in eyes enucleated from the Collaborative Ocular Melanoma Study. COMS report no. 6.* Am J Ophthalmol, 1998. **125**(6): p. 745-66.
41. Kaliki, S. and C.L. Shields, *Uveal melanoma: relatively rare but deadly cancer.* Eye (Lond), 2017. **31**(2): p. 241-257.
42. Alsafadi, S., et al., *Cancer-associated SF3B1 mutations affect alternative splicing by promoting alternative branchpoint usage.* Nat Commun, 2016. **7**: p. 10615.
43. Sisley, K., et al., *Non-random abnormalities of chromosomes 3, 6, and 8 associated with posterior uveal melanoma.* Genes Chromosomes Cancer, 1992. **5**(3): p. 197-200.
44. van den Bosch, T., et al., *Higher percentage of FISH-determined monosomy 3 and 8q amplification in uveal melanoma cells relate to poor patient prognosis.* Invest Ophthalmol Vis Sci, 2012. **53**(6): p. 2668-74.
45. Mooy, C., et al., *DNA flow cytometry in uveal melanoma: the effect of pre-enucleation irradiation.* Br J Ophthalmol, 1995. **79**(2): p. 174-7.
46. Pilarski, R., et al., *BAP1 Tumor Predisposition Syndrome*, in *GeneReviews((R))*, M.P. Adam, et al., Editors. 1993: Seattle (WA).
47. Stalhammar, G. and H.E. Grossniklaus, *Intratumor Heterogeneity in Uveal Melanoma BAP-1 Expression.* Cancers (Basel), 2021. **13**(5).
48. Herrspiegel, C., et al., *Digital morphometry of tumor nuclei correlates to BAP-1 status, monosomy 3, gene expression class and survival in uveal melanoma.* Exp Eye Res, 2020. **193**: p. 107987.
49. Zhou, R. and R.R. Caspi, *Ocular immune privilege.* F1000 Biol Rep, 2010. **2**.
50. McKenna, K.C. and P.W. Chen, *Influence of immune privilege on ocular tumor development.* Ocul Immunol Inflamm, 2010. **18**(2): p. 80-90.
51. Meecham, W.J., D.H. Char, and S. Kaleta-Michaels, *Infiltrating lymphocytes and antigen expression in uveal melanoma.* Ophthalmic Res, 1992. **24**(1): p. 20-6.
52. Bronkhorst, I.H., et al., *Detection of M2-macrophages in uveal melanoma and relation with survival.* Invest Ophthalmol Vis Sci, 2011. **52**(2): p. 643-50.
53. Wierenga, A.P.A., et al., *Soluble HLA in the Aqueous Humour of Uveal Melanoma Is Associated with Unfavourable Tumour Characteristics.* Cancers (Basel), 2019. **11**(8).

54. Souri, Z., et al., *HLA Expression in Uveal Melanoma: An Indicator of Malignancy and a Modifiable Immunological Target.* Cancers (Basel), 2019. **11**(8).
55. Greten, F.R. and S.I. Grivennikov, *Inflammation and Cancer: Triggers, Mechanisms, and Consequences.* Immunity, 2019. **51**(1): p. 27-41.
56. Makitie, T., et al., *Microvascular density in predicting survival of patients with choroidal and ciliary body melanoma.* Invest Ophthalmol Vis Sci, 1999. **40**(11): p. 2471-80.
57. Usui, Y., et al., *Aqueous immune mediators in malignant uveal melanomas in comparison to benign pigmented intraocular tumors.* Graefes Arch Clin Exp Ophthalmol, 2017. **255**(2): p. 393-399.
58. He, Y.G., et al., *Expression and possible function of IL-2 and IL-15 receptors on human uveal melanoma cells.* Invest Ophthalmol Vis Sci, 2004. **45**(12): p. 4240-6.
59. Repp, A.C., et al., *Human uveal melanoma cells produce macrophage migration-inhibitory factor to prevent lysis by NK cells.* J Immunol, 2000. **165**(2): p. 710-5.
60. Niederkorn, J.Y., *Immune escape mechanisms of intraocular tumors.* Prog Retin Eye Res, 2009. **28**(5): p. 329-47.
61. Poulet, G., J. Massias, and V. Taly, *Liquid Biopsy: General Concepts.* Acta Cytol, 2019. **63**(6): p. 449-455.
62. Macias, M., et al., *Liquid Biopsy: From Basic Research to Clinical Practice.* Adv Clin Chem, 2018. **83**: p. 73-119.
63. Im, D.H., et al., *Potential of Aqueous Humor as a Liquid Biopsy for Uveal Melanoma.* Int J Mol Sci, 2022. **23**(11).
64. Tomar, U., et al., *Liquid biopsy and its significance in tumour - Detection in the field of pathology.* J Oral Maxillofac Pathol, 2023. **27**(1): p. 195-200.
65. Chu, D. and B.H. Park, *Liquid biopsy: unlocking the potentials of cell-free DNA.* Virchows Arch, 2017. **471**(2): p. 147-154.
66. Ding, Z., et al., *Proteomics technologies for cancer liquid biopsies.* Mol Cancer, 2022. **21**(1): p. 53.
67. Forler, S., O. Klein, and J. Klose, *Individualized proteomics.* J Proteomics, 2014. **107**: p. 56-61.
68. Jin, E. and J.V. Burnier, *Liquid Biopsy in Uveal Melanoma: Are We There Yet?* Ocul Oncol Pathol, 2021. **7**(1): p. 1-16.
69. de Bruyn, D.P., et al., *Is Tissue Still the Issue? The Promise of Liquid Biopsy in Uveal Melanoma.* Biomedicines, 2022. **10**(2).
70. Midena, E., et al., *In vivo intraocular biomarkers: Changes of aqueous humor cytokines and chemokines in patients affected by uveal melanoma.* Medicine (Baltimore), 2020. **99**(38): p. e22091.
71. Midena, G., et al., *Chorioretinal Side Effects of Therapeutic Ocular Irradiation: A Multimodal Imaging Approach.* J Clin Med, 2020. **9**(11).
72. Zemba, M., et al., *Ocular Complications of Radiotherapy in Uveal Melanoma.* Cancers (Basel), 2023. **15**(2).

73. Midena, E., et al., *The effect of external eye irradiation on choroidal circulation.* Ophthalmology, 1996. **103**(10): p. 1651-60.
74. Parrozzani, R., et al., *IDENTIFICATION AND CLASSIFICATION OF MACULAR MORPHOLOGIC BIOMARKERS RELATED TO VISUAL ACUITY IN RADIATION MACULOPATHY: A Multimodal Imaging Study.* Retina, 2020. **40**(7): p. 1419-1428.
75. Frizziero, L., et al., *Intravitreal dexamethasone implant in radiation-induced macular oedema.* Br J Ophthalmol, 2017. **101**(12): p. 1699-1703.
76. Parrozzani, R., et al., *Peripapillary vascular changes in radiation optic neuropathy: an optical coherence tomography angiography grading.* Br J Ophthalmol, 2018. **102**(9): p. 1238-1243.
77. Gabriele, M.L., et al., *Optical coherence tomography: history, current status, and laboratory work.* Invest Ophthalmol Vis Sci, 2011. **52**(5): p. 2425-36.
78. Wolf, S. and U. Wolf-Schnurrbusch, *Spectral-domain optical coherence tomography use in macular diseases: a review.* Ophthalmologica, 2010. **224**(6): p. 333-40.
79. Parrozzani, R., et al., *RADIATION MACULOPATHY IS ANTICIPATED BY OCT HYPERREFLECTIVE RETINAL FOCI: A Large, Prospective, Confirmation Study.* Retina, 2022. **42**(4): p. 752-759.
80. Ly, L.V., et al., *Inflammatory cytokines in eyes with uveal melanoma and relation with macrophage infiltration.* Invest Ophthalmol Vis Sci, 2010. **51**(11): p. 5445-51.
81. Smit, K.N., et al., *Combined mutation and copy-number variation detection by targeted next-generation sequencing in uveal melanoma.* Mod Pathol, 2018. **31**(5): p. 763-771.
82. Sarubi, H.C., et al., *Molecular and immunohistochemical analyses of uveal melanoma patient cohort.* Melanoma Res, 2019. **29**(3): p. 248-253.
83. Wierenga, A.P.A., et al., *Aqueous Humor Biomarkers Identify Three Prognostic Groups in Uveal Melanoma.* Invest Ophthalmol Vis Sci, 2019. **60**(14): p. 4740-4747.
84. Scholes, A.G., et al., *Monosomy 3 in uveal melanoma: correlation with clinical and histologic predictors of survival.* Invest Ophthalmol Vis Sci, 2003. **44**(3): p. 1008-11.
85. Maat, W., et al., *Monosomy of chromosome 3 and an inflammatory phenotype occur together in uveal melanoma.* Invest Ophthalmol Vis Sci, 2008. **49**(2): p. 505-10.
86. Oliva, M., A.J. Rullan, and J.M. Piulats, *Uveal melanoma as a target for immune-therapy.* Ann Transl Med, 2016. **4**(9): p. 172.
87. Dunavoelgyi, R., et al., *Intraocular activation of angiogenic and inflammatory pathways in uveal melanoma.* Retina, 2012. **32**(7): p. 1373-84.
88. Gezgin, G., et al., *Genetic evolution of uveal melanoma guides the development of an inflammatory microenvironment.* Cancer Immunol Immunother, 2017. **66**(7): p. 903-912.

89. Cheng, Y., et al., *Cytokines concentrations in aqueous humor of eyes with uveal melanoma.* Medicine (Baltimore), 2019. **98**(5): p. e14030.
90. Kalirai, H., et al., *Lack of BAP1 protein expression in uveal melanoma is associated with increased metastatic risk and has utility in routine prognostic testing.* Br J Cancer, 2014. **111**(7): p. 1373-80.
91. van Poppelen, N.M., et al., *Genetics of Ocular Melanoma: Insights into Genetics, Inheritance and Testing.* Int J Mol Sci, 2020. **22**(1).
92. Tate, J.G., et al., *COSMIC: the Catalogue Of Somatic Mutations In Cancer.* Nucleic Acids Res, 2019. **47**(D1): p. D941-D947.
93. Koopmans, A.E., et al., *Clinical significance of immunohistochemistry for detection of BAP1 mutations in uveal melanoma.* Mod Pathol, 2014. **27**(10): p. 1321-30.
94. Shah, A.A., T.D. Bourne, and R. Murali, *BAP1 protein loss by immunohistochemistry: a potentially useful tool for prognostic prediction in patients with uveal melanoma.* Pathology, 2013. **45**(7): p. 651-6.
95. Szalai, E., et al., *Uveal Melanoma Nuclear BRCA1-Associated Protein-1 Immunoreactivity Is an Indicator of Metastasis.* Ophthalmology, 2018. **125**(2): p. 203-209.
96. Tabuenca Del Barrio, L., et al., *Prognostic Factor Utility of BAP1 Immunohistochemistry in Uveal Melanoma: A Single Center Study in Spain.* Cancers (Basel), 2021. **13**(21).
97. van de Nes, J.A., et al., *Comparing the Prognostic Value of BAP1 Mutation Pattern, Chromosome 3 Status, and BAP1 Immunohistochemistry in Uveal Melanoma.* Am J Surg Pathol, 2016. **40**(6): p. 796-805.
98. Ewens, K.G., et al., *Chromosome 3 status combined with BAP1 and EIF1AX mutation profiles are associated with metastasis in uveal melanoma.* Invest Ophthalmol Vis Sci, 2014. **55**(8): p. 5160-7.
99. Midena, E., et al., *OCT Hyperreflective Retinal Foci in Diabetic Retinopathy: A Semi-Automatic Detection Comparative Study.* Front Immunol, 2021. **12**: p. 613051.
100. Frizziero, L., et al., *Hyperreflective Intraretinal Spots in Radiation Macular Edema on Spectral Domain Optical Coherence Tomography.* Retina, 2016. **36**(9): p. 1664-9.
101. Vujosevic, S., et al., *HYPERREFLECTIVE RETINAL SPOTS IN NORMAL AND DIABETIC EYES: B-Scan and En Face Spectral Domain Optical Coherence Tomography Evaluation.* Retina, 2017. **37**(6): p. 1092-1103.
102. Midena, E., E. Pilotto, and S. Bini, *Hyperreflective Intraretinal Foci as an OCT Biomarker of Retinal Inflammation in Diabetic Macular Edema.* Invest Ophthalmol Vis Sci, 2018. **59**(13): p. 5366.
103. Vujosevic, S., et al., *Aqueous Humor Biomarkers of Muller Cell Activation in Diabetic Eyes.* Invest Ophthalmol Vis Sci, 2015. **56**(6): p. 3913-8.

104. Sarthy, V., *Focus on molecules: glial fibrillary acidic protein (GFAP).* Exp Eye Res, 2007. **84**(3): p. 381-2.
105. Vujosevic, S., et al., *Proteome analysis of retinal glia cells-related inflammatory cytokines in the aqueous humour of diabetic patients.* Acta Ophthalmol, 2016. **94**(1): p. 56-64.
106. Frizziero, L., et al., *Subthreshold Micropulse Laser Modulates Retinal Neuroinflammatory Biomarkers in Diabetic Macular Edema.* J Clin Med, 2021. **10**(14).